

JAMES | Journal of Advances in Modeling Earth Systems*



RESEARCH ARTICLE

10.1029/2021MS002917

Special Section:

Using radiative-convective equilibrium to understand convective organization, clouds, and tropical climate

Key Points:

- Controls of high and mid-level clouds are independent of whether a model employs parameterized or explicit convection
- The response of anvil cloud fraction to a warming surface and more stable troposphere is highly controlled by radiatively-driven divergence
- Mid-level clouds robustly decrease with warming due to integrated cooling increasing slower than convective heat flux

Supporting Information:

Supporting Information may be found in the online version of this article.

Correspondence to:

C. L. Stauffer, cls14b@fsu.edu

Citation:

Stauffer, C. L., & Wing, A. A. (2022). Properties, changes, and controls of deep-convecting clouds in radiative-convective equilibrium. Journal of Advances in Modeling Earth Systems, 14, e2021MS002917. https://doi.org/10.1029/2021MS002917

Received 23 NOV 2021 Accepted 7 JUN 2022

© 2022 The Authors. Journal of Advances in Modeling Earth Systems published by Wiley Periodicals LLC on behalf of American Geophysical Union. This is an open access article under the terms of the Creative Commons Attribution License, which permits use, distribution and reproduction in any medium, provided the original work is properly cited.

Properties, Changes, and Controls of Deep-Convecting Clouds in Radiative-Convective Equilibrium

Catherine L. Stauffer¹ and Allison A. Wing¹

¹Department of Earth, Ocean and Atmospheric Science, Florida State University, Tallahassee, FL, USA

Abstract Changes in tropical high clouds associated with deep convection with warming are one of the largest sources of uncertainty in climate feedbacks. Here, we leverage an ensemble of models of many types in an idealized configuration to investigate how and why high clouds change the way they do. We find that deep-convecting anvils, independent of how cloud fraction is defined, increase in height, increase slightly in temperature, and (generally) decrease in cloud fraction with warming sea surface temperature (SST). The controls on anvil height and temperature have well established physical reasoning, but the response of anvil cloud fraction to warming is more variable across studies and not as well understood. We test a previously published hypothesis for control of anvil coverage and find that, at least to first order, it is highly controlled by radiatively-driven divergence, in which, with warming, anvil clouds occur in a more stable environment requiring less divergence to balance radiative cooling and, therefore, decreasing cloud coverage. We also find mid-level clouds robustly decrease in coverage with warming SST and can be represented by a diagnostic scaling which attributes the robust decrease in mid-level clouds to the rapid increase in the overall convective heating of the clouds compared to the much slower increase in the integrated radiative cooling rate. The robust response of deep-convective clouds to warming and support for the underlying physical mechanisms across the spectrum of models, with both explicit and parameterized convection, increases confidence in their contribution to climate feedbacks.

Plain Language Summary Tropical thunderstorm clouds are affected by a changing climate and can further modulate climate in different and contradictory ways. However, the exact impact on climate is highly uncertain due to their competing effects of cooling and warming the Earth's surface. In this study, we seek to improve our understanding of what determines how these tropical clouds respond to a warming surface by looking for consistent results across over 30 different types of models. We find that the high clouds increase in altitude, slightly increase in temperature, and decrease in coverage for most of the models. We also determine that the high clouds change largely due to a circulation driven by the effects of clear sky regions.

1. Introduction

Clouds are the biggest source of uncertainty in estimates of climate sensitivity (Bony et al., 2015; Boucher et al., 2014; Dufresne & Bony, 2008; Vial et al., 2013; Zelinka et al., 2020). There has been some progress in constraining the equilibrium climate sensitivity (Sherwood et al., 2020) but different types of clouds contribute different feedbacks, often in competition with one another. Cloud feedbacks are contributed by changes in cloud amount, altitude, optical depth, and type of cloud (Thorsen et al., 2018; Yue et al., 2016; Zelinka et al., 2012, 2013, 2016; Zhou et al., 2013). Upward shifts in high clouds contribute a positive feedback (Hartmann & Larson, 2002; Zelinka & Hartmann, 2010) as does a reduction in low-level tropical cloud (Bretherton, 2015; Rieck et al., 2012). A negative shortwave feedback, however, is introduced when high latitude low-level clouds have an increase in optical depth (Ceppi et al., 2016; Gordon & Klein, 2014; McCoy et al., 2015). It is agreed that there is a net positive cloud feedback (Boucher et al., 2014; Ceppi & Nowack, 2021; Ceppi et al., 2017; Zelinka et al., 2016), but its magnitude remains uncertain. Tropical anvil clouds, in particular, are now recognized to represent the largest uncertainty in climate feedback estimates as a whole (Sherwood et al., 2020). This is mainly because of the large uncertainty in how these clouds change with warming (Bony et al., 2006; Boucher et al., 2014; Kodama et al., 2021; Zelinka et al., 2020). While models with explicit convection have provided insights on cloud processes (Bretherton & Blossey, 2014; Bretherton et al., 2013; Rieck et al., 2012), estimates of cloud feedbacks have overwhelmingly been performed in models with parameterized convection, primarily CMIP-type models (Boucher et al., 2014; Eyring et al., 2016). With few exceptions, the proper calculation of cloud feedbacks has not been accomplished using models with explicit convection, which have typically only

STAUFFER AND WING 1 of 23



examined changes in the cloud radiative effect. Even for the few studies that have studied the response of clouds to warming in greater detail, such as cloud optical properties (Ohno & Satoh, 2018; Ohno et al., 2019, 2021), using radiative kernel corrections (Cronin & Wing, 2017), or in some super-parameterized models (Blossey et al., 2009; Stan & Xu, 2014; Wyant et al., 2009) further decomposition is limited or absent, and certainly not as extensive as in the CMIP-type models. There is thus a continued and urgent need for further investigation into mechanisms for the changes in tropical deep-convective clouds with warming and the contribution of clouds to climate feedbacks, especially in models that simulate convection explicitly.

Although the contribution of anvil clouds to the climate feedback may still be uncertain, several features of deep-convecting tropical clouds and their changes with warming sea surface temperature (SST) are well understood, based on idealized modeling and observations. Radiative-convective equilibrium (RCE) is a simplified framework of the tropical atmosphere characterized by a statistical balance between radiative cooling and convective heating (Held et al., 1993) and is frequently used to study tropical convection and climate sensitivity. Using RCE, the temperature of deep-convecting anvil clouds has been found to remain approximately fixed as the surface temperature changes, arising from a simple thermodynamic constraint on the radiative cooling profile by the Clausius Clapeyron relationship (Hartmann & Larson, 2002), a feature referred to as the "Fixed Anvil Temperature" hypothesis, or FAT. An analytical theory for why FAT occurs at around 220 K showed that, in addition to Clausius Clapeyron, the distribution of H₂O absorption coefficients are among the ingredients for FAT (Jeevanjee & Fueglistaler, 2020). Zelinka and Hartmann (2010) revised the FAT hypothesis to consider a slight increase in anvil temperature due to an increase in static stability in the upper troposphere in warmer climates ("Proportionally Higher Anvil Temperature," or PHAT). Although most studies find that anvil temperature increases slightly or remains fixed with warming SST (e.g., Kuang & Hartmann, 2007), the assumptions underlying FAT have recently been questioned and control of anvil clouds remains a subject of ongoing work (Seeley, Jeevanjee, Langhans, & Romps, 2019; Seeley, Jeevanjee, & Romps, 2019).

While the (near-) isothermal rise of cloud tops has a sound hypothesis with robust physical reasoning, the change in anvil coverage with warming is less consistent. Some studies find that anvil coverage decreases with warming (e.g., Bony et al., 2016; Cronin & Wing, 2017; Kuang & Hartmann, 2007; Tompkins & Craig, 1999) while others find it increases (e.g., Chen et al., 2016; Noda et al., 2019; Ohno & Satoh, 2018; Ohno et al., 2019; Singh & O'Gorman, 2015; Tsushima et al., 2014). This begs the question of what mechanistically is controlling cloud fraction and can it explain the varied results? Bony et al. (2016) proposed that the mechanisms controlling anvil coverage are fundamentally the same thermodynamic constraints that control cloud top height and temperature. By mass continuity, the divergence of the upward deep-convective mass flux, and therefore anvil spreading (what we are interested in), is constrained by the vertical divergence of clear sky subsidence. In the clear-sky region there is a balance between radiative cooling and warming by subsidence, so the level of peak radiatively-driven divergence (R_D) is where the radiative cooling rate drops off drastically following the Clausius-Clapeyron dependence of water vapor, the primary longwave emitter.

Bony et al. (2016) found that anvil cloud fraction and R_D decrease together with warming temperature. This relationship was found in general circulation models (GCMs) in RCE, simulations with aggregated and un-aggregated convection, non-RCE states (Bony et al., 2016), in a cloud resolving model (CRM, Cronin & Wing, 2017), and observations (Zelinka & Hartmann, 2011), suggesting that it is a fundamental property. In particular, Bony et al. (2016) argued that an increase in static stability is required to necessarily decrease the pressure for a FAT scenario or increase the temperature necessary for a PHAT scenario which results in less subsidence (and thus, R_D) needed to balance radiative cooling, and thus a decrease in anvil coverage. They referred to the decrease in anvil coverage, which allows for more longwave cooling to space, as a "stability iris."

RCE offers a framework for studying tropical deep-convecting clouds, and their response to warming, in the absence of complication by heterogeneous boundary conditions or forcing and the resulting dynamical instabilities. RCE is a powerful tool because it has connections to theory, analytic models, as well as representing elements of the real Earth system such as similarities to the tropical atmosphere at large spatial and temporal scales (Jakob et al., 2019; Miyakawa et al., 2022). The simplicity of RCE also allows for its configuration to be used by a variety of types of models and at a relatively low computation cost. The Radiative Convective Equilibrium Model Intercomparison Project (RCEMIP, Wing et al., 2018, 2020) takes advantage of the simplicity of RCE by having representation from CRMs, GCMs, global cloud resolving models (GCRMs), and large eddy simulations (LES), all configured in a common framework.

STAUFFER AND WING 2 of 23



Wing et al. (2020) found that the RCEMIP models simulate a wide range of profiles of cloud fraction and other significant climate variables. Nearly all models exhibit self-aggregation of convection, which is a well documented instability of the RCE state, defined by Wing et al. (2017) as the spontaneous organization of convection despite homogeneous boundary conditions and forcing. RCEMIP models agree that self-aggregation reduces the extent of high clouds, dries the mean state, and allows for more efficient radiative cooling. This has implications for the spread in climate sensitivity across RCEMIP, which is explained in part by the response of aggregation to warming, for which there is no consensus across models (Becker & Wing, 2020). However, there is a consensus on how anvil clouds change with warming SST. In agreement with expectations from the prior work discussed above, Wing et al. (2020) found that anvil clouds increase in height and slightly increase in temperature with warming, as well as decrease in coverage in most of the models.

The RCEMIP models are configured in a consistent manner, with the same SST, solar insolation, trace gas profiles, and (within a type of model) domain size and resolution; yet, there is a wide range in how key climate variables are simulated (Wing et al., 2020). This is unsurprising when one considers the properties that make each model unique and are not a part of the controlled configuration of RCE (such as microphysics, convection schemes, and dynamical cores). However, the strength of RCEMIP lies in this very characteristic; that certain consistent properties arise from such a diverse suite of models provides an opportunity to understand what drives these robust behaviors. And, although idealized frameworks such as RCE highly simplify the physics of the climate system, many properties predicted by RCE are also found in more complex models or in observations of the tropical atmosphere (Hartmann et al., 2019). For example, Holloway et al. (2017) reviewed observational studies of convective aggregation that found similar relationships to those seen in RCE simulations of self-aggregation.

This work will expand upon the analysis of Wing et al. (2020) to examine how deep-convective clouds change with warming in more detail and test hypotheses from the literature for the control of these clouds. RCEMIP is a powerful tool because it is the first time such a large (30+) collection of models of many types have been consistently configured in RCE, thus providing a more comprehensive test of changes in deep-convective clouds and their mechanisms than previously possible. Section 2 will briefly overview the data set as well as the methods for calculating the various metrics used in this study, Section 3 will overview what the cloud profiles look like and how cloud fraction behaves for an alternative definition of cloud fraction, Section 4 tests a hypothesis for the control of anvil clouds, and Section 5 will describe the changes in mid-level clouds and test a method of analyzing their controls.

2. Data Set and Methods

2.1. Model Configuration

RCEMIP (Wing et al., 2018, 2020) consists of over 30 models including CRMs, GCMs, GCRMs, and LES. These models are all consistently configured as idealized simulations (e.g., aquaplanet, uniform insolation, uniform SST, no rotation) of RCE, which is a simplified view of the tropical atmosphere where, on average, radiative cooling balances convective heating. The simulations are run at three different SSTs (295, 300, and 305 K) to simulate different climates and on a "large" domain (RCE_large) that allows self-aggregation of convection to occur as well as a "small" domain (RCE_small) that resists self-aggregation. RCE_small simulations are initialized everywhere with the same analytic sounding (Wing et al., 2018) and RCE_large simulations are initialized everywhere with an equilibrium sounding from the corresponding RCE_small simulation.

The CRMs have approximately 74 vertical levels where RCE_small has horizontal dimensions of $\sim 100 \times 100 \text{ km}^2$ with 1 km grid spacing and RCE_large is $\sim 6000 \times 400 \text{ km}^2$ with 3 km grid spacing. They are run for 100 days. The CRM-VERT simulations have the same horizontal configuration as RCE_small CRM simulations but have ~ 146 vertical levels. The CRM-LES simulations are run for 50 days with the same vertical grid as the CRM-VERT simulations but a horizontal grid spacing of 200 m. The GCRM simulations have 74 vertical levels and 3–4 km grid spacing, similar to the resolution of the CRM simulations. For computational efficiency, they are run with a reduced Earth radius for 100 days. The spherical GCM simulations are configured using their CMIP6 (Eyring et al., 2016) vertical and horizontal settings and are run for $\sim 1,000$ days. The WRF-GCM simulations have a horizontal resolution of 50 km with GCM physics but on the CRM Cartesian grid.

More information on the RCEMIP data set is provided by Wing et al. (2018); Wing et al. (2020).

STAUFFER AND WING 3 of 23



2.2. Cloud Fraction

Originally, the RCEMIP protocol (Wing et al., 2018) called for diagnostic cloud fraction to be based on defining the presence of cloud using a threshold value of $cw + ci > \min(0.01q_{sw}, 10^{-5}gg^{-1})$ or the output of a cloud scheme for models employing such a scheme (cfv0), where cw is the cloud liquid water condensate, ci is the cloud ice condensate, and q_{sw} is the saturation mixing ratio over water. However, subsequent to Wing et al. (2020), it was determined that this definition was not consistently applied across the participating models. Consequently, this paper recalculates cloud fraction from available 3D data using 1: the RCEMIP protocol definition (Wing et al., 2018) applied consistently to the models with explicit convection (cfv1, see Appendix A and Text S1 in Supporting Information S1) and 2: a less-generous definition which uses a cloud water condensate threshold value of 10⁻⁵ gg⁻¹ (cfv2, see Appendix A and Section 3), which is the definition used in the remainder of this paper. cfv1 and cfv2 are applied only to models with explicit convection due to the use of 3D output data and it not being appropriate to diagnose a GCM grid cell as completely cloudy or clear based on its output value of cloud condensate on a grid on order of 1°. Therefore, we continue to use the model-provided cloud fraction from the cloud scheme for models with parameterized convection. We analyze the equilibrium state by considering averages in time excluding the first 75 days of the simulation which are derived from six-hourly instantaneous snapshots. Appendix A goes into further detail on the calculation of cfv1 and cfv2 and demonstrates that the previously mentioned time sampling is sufficient to generate representative time- and domain-mean profiles while the consistently applied definition of cfv2 allows for a fairer comparison of cloud properties across models.

2.3. Radiatively-Driven Divergence

One objective of this study is to test the extent to which radiatively-driven divergence controls anvil cloud fraction, as argued by Bony et al. (2016). Following Bony et al. (2016) (see also Cronin & Wing, 2017), radiatively-driven divergence (R_D) is defined using the following:

$$R_D = \frac{\partial \omega}{\partial P} \tag{1}$$

$$\omega = -\frac{Q_r}{S} \tag{2}$$

$$S = -\frac{T}{\theta} \frac{\partial \theta}{\partial P} \tag{3}$$

where R_D is the radiatively-driven divergence in day⁻¹, ω is the clear-sky radiatively-driven vertical motion in units of Pa s⁻¹, P is the pressure with units Pa, Q_r is the clear-sky radiative cooling rate with units K s⁻¹, S is static stability with units K Pa⁻¹, T is the temperature in K, and θ is the potential temperature in K. Since the location of the anvil is expected to be tied to the location of the peak R_D , the upper-level maximum in R_D is compared to the anvil peak.

Three versions of R_D are calculated using domain-mean equilibrium profiles of temperature, pressure, and clear-sky radiative cooling rate. R_D is the "standard" version of the calculation using Equation 1. The other two versions are calculated to test the relative contributions of changes in clear-sky radiative cooling and static stability to changes in R_D . This is accomplished by eliminating variability in Q_r and S across SSTs by individually holding the properties constant at their 300 K value. In other words, what is the tendency of R_D when static stability does not change with SST (R_{D300S}) and, similarly, what is the tendency of R_D when the clear-sky radiative cooling rate does not change with SST (R_{D300O})?

2.4. Mid-Level Cloud Fraction

2.4.1. Mid-Level Metrics

In Section 5 we assess the response of mid-level clouds to warming and test the extent to which the profiles across simulations at different SSTs collapse when temperature is used as a vertical axis. In order to quantify this property, we define four key metrics using the process below across all models:

STAUFFER AND WING 4 of 23

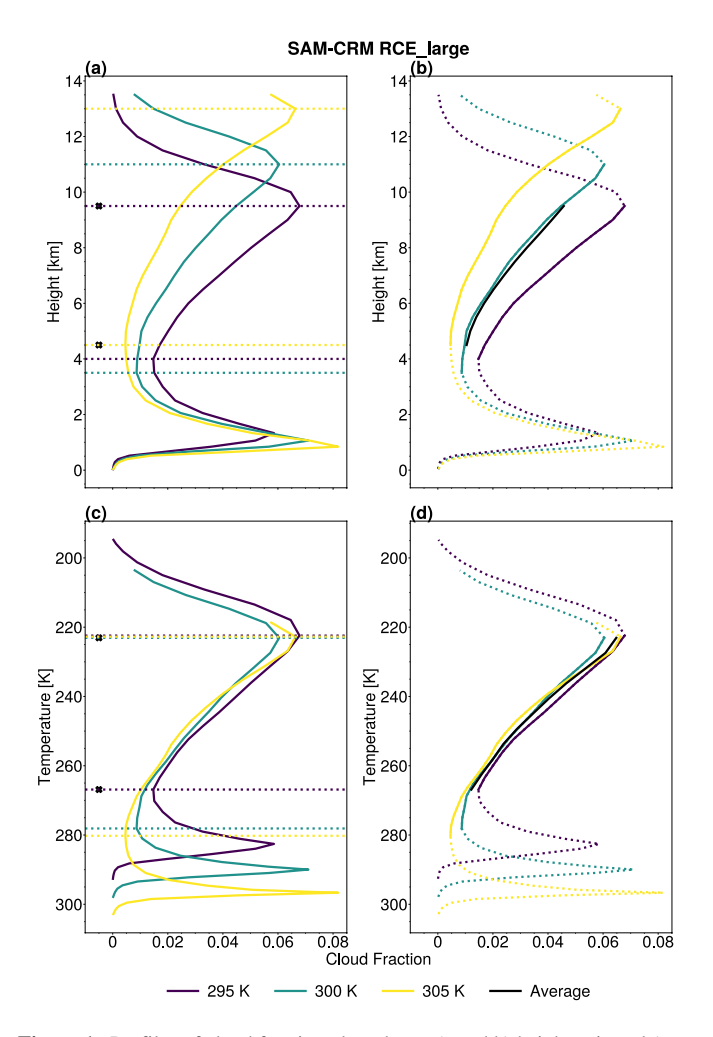


Figure 1. Profiles of cloud fraction plotted on a (a and b) height axis and (c and d) temperature axis. The left column contains the unaltered profiles, the horizontal lines are the locations of the mid-level minimum and upper-level maximum for each profile, the black X shows the "absolute" mid-level region used in the analysis. The right column contains the profiles interpolated to the restricted *z*-axis defined by the Xs in the left column as solid lines, the average cloud fraction profile across the sea surface temperatures in black, and the original unaltered cloud fraction profile as dotted lines.

- Define the mid-level region (dashed horizontal lines in Figures 1a and 1c): the region between the mid-level minimum in cloud fraction (between the lower-level and upper-level peaks in cloud fraction) and the upper-level maximum in cloud fraction individually for each SST.
- 2. Define the new height axis (black "x"s in Figure 1a): the region between the maximum height of the mid-level cloud fraction minimum across SSTs and the minimum height of the upper-level cloud fraction maximum across the SSTs ($Z_{avg} = max(Z_{mid}(295), Z_{mid}(300), Z_{mid}(305))$): $min(Z_{top}(295), Z_{top}(300), Z_{top}(305)))$).
- 3. Define the new temperature axis (black "x"s in Figure 1c): the region between the minimum temperature of the mid-level cloud fraction minimum across SSTs and the maximum temperature of the upper-level cloud fraction maximum across the SSTs ($T_{\rm avg} = \min(T_{\rm mid}(295), T_{\rm mid}(300), T_{\rm mid}(305))$): $\max(T_{\rm top}(295), T_{\rm top}(300), T_{\rm top}(305)))$).
- 4. Interpolate cloud fraction profiles to T_{avg} and Z_{avg} , common axes across all SSTs for a given model.
- 5. Compute the following metrics where (A) is the average over the interpolated mid-level region, following Equation 4, where c1 and c2 are the mid-level bounds in a given vertical coordinate (Z or T):

$$\langle A \rangle = \frac{\int_{c_1}^{c_2} A dc}{\int_{c_1}^{c_2} dc} \tag{4}$$

- $\langle CF_{avg} \rangle$; where $CF_{avg} = \text{mean}(CF(295), CF(300), CF(305))$.
- $\langle CF_{\text{range}} \rangle$; where $CF_{\text{range}} = \max(CF(295), CF(300), CF(305)) \min(CF(295), CF(300), CF(305)).$
- $\langle CF_{\Delta} \rangle$; where $CF_{\Delta} = CF(305) CF(295)$.

This example was for cloud fraction, other variables used in our analysis are similarly interpolated and averaged using the new temperature and height axes restricted by the mid-level cloud fraction region. We note that Abbott et al. (2020) used a method similar in concept to $\langle CF_{\rm range} \rangle$ to measure the collapse of a profile between two coordinates with a single metric.

2.4.2. Mid-Level Scaling

Following Cronin and Wing (2017), we test a diagnostic scaling for mid-level cloud fraction based on the approximation that mid-level cumulus convective enthalpy flux, $(F_c = \sigma_c w_c [L_v \rho_v^* (1 - RH) + \delta s])$, is balanced by radiative cooling of the troposphere above $\left(Q = \int_{T_T}^T J(T') dT'\right)$, where J(T) is the radiative cooling rate and is integrated from a level up to the tropopause, σ_c is the cloud fraction (using cfv2), w_c is the in-cloud vertical velocity (the

vertical velocity co-located with cloudy pixels following the threshold of cfv2), $L_v \rho_v^* (1-RH)$ is the latent heat excess per unit volume carried upward by clouds relative to the subsiding unsaturated environment, RH is relative humidity, $\rho_v^* = e^*/(R_vT)$ is the saturation vapor density, and δs is the dry static energy excess per unit volume carried upward by clouds. $\delta s = 1004*(\delta s_{cor} - \delta s_{down})*\rho$ where δs_{cor} is wherever the virtual temperature is greater than the horizontal average of virtual temperature in a strong updraft $(w > 2 ms^{-1})$ and δs_{down} is wherever the virtual temperature is less than the horizontal average of virtual temperature in a strong downdraft $(w < -2 ms^{-1})$. We calculate each of these quantities from the instantaneous 3D data, for those models with explicit convection for which it is available. Solving for cloud fraction, σ_c , results in Equation 5 (see also Equation 5 of Cronin & Wing, 2017).

$$\sigma_c(T) = \frac{\int_{T_T}^T J(T') dT'}{w_c \left[L_v \rho_v^* (1 - RH) + \delta s \right]}$$
 (5)

STAUFFER AND WING 5 of 23



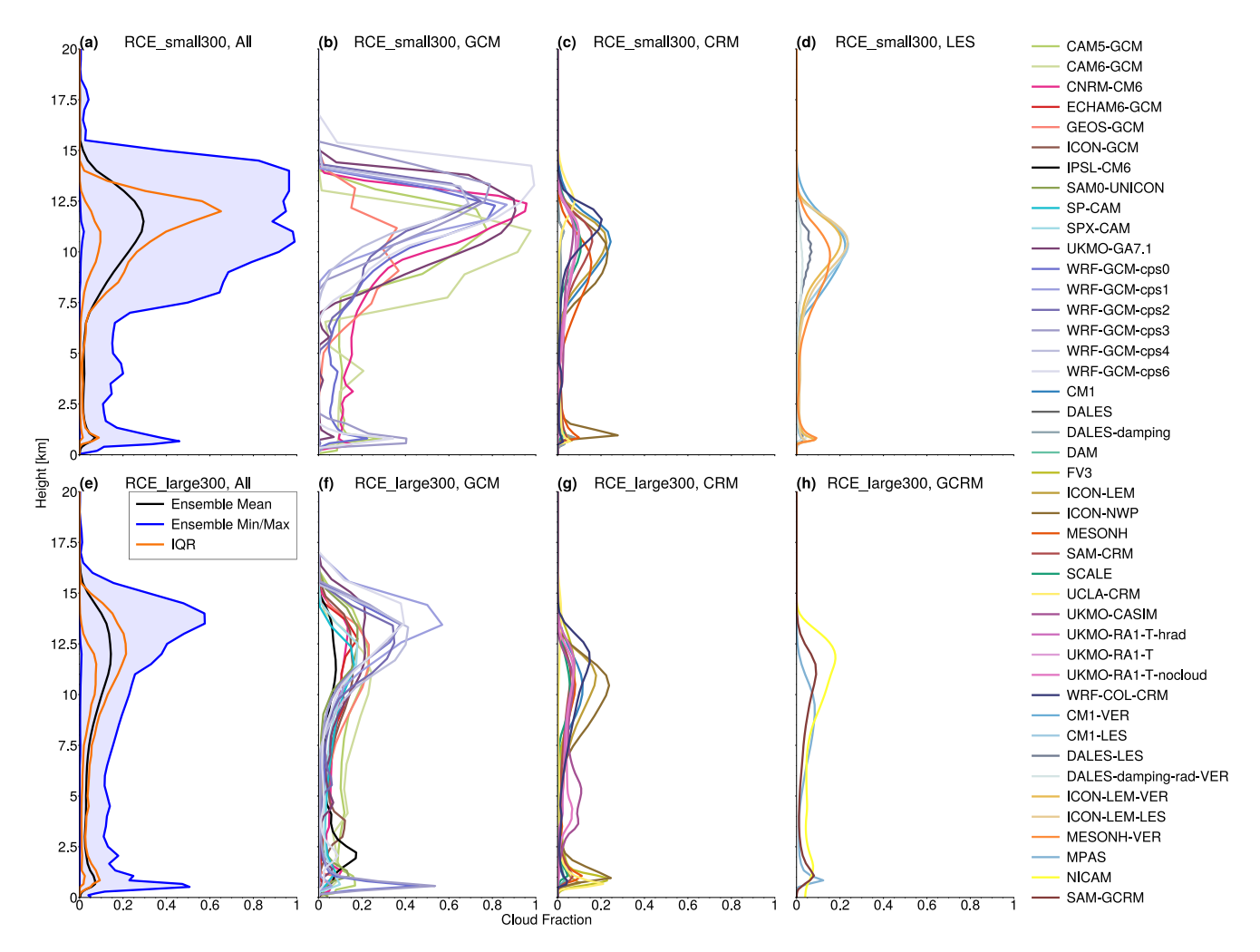


Figure 2. Horizontally- and temporally-averaged profiles of cfv2 for RCE_small (top row: a, b, c, and d) and RCE_large (bottom row: e, f, g, and h) simulations at 300 K. The first column (a and e) represents the range of the profiles of all the models in blue shading, the orange lines are the interquartile range of the data, and the black line is the mean across the models. The remaining columns are the individual profiles for the models with parameterized convection (b and f), cloud resolving models (c and g), and large eddy simulations and global cloud resolving model simulations (d and h, respectively). This figure is modeled after Figure 9 in Wing et al. (2020) where panels (b and f) are identical to those in Wing et al. (2020) (and in Figure S1 in Supporting Information S1 of this paper).

3. Changes in Anvil Properties With Warming SST

As previously mentioned, we re-calculated cloud fraction for two reasons; 1: to consistently apply a single definition across all of the models with explicit convection and 2: to test whether including saturation mixing ratio over water in the cloud condensate threshold was too generous of a threshold and needed to be corrected. The latter results in two notable and important differences in anvil cloud properties with the exclusion of $q_{s,w}$.

First, cfv2 has less high cloud (Figure 2) than cfv0 (Figure 9 of Wing et al., 2020) or cfv1 (Figure S1 in Supporting Information S1). There is an average decrease in anvil cloud fraction from cfv1 to cfv2 of 0.527 (which is quite large) in the RCE_large models with explicit convection (where the new definition applies) and an average decrease of 0.514 in all but five (of 22) of the RCE_small models with explicit convection, confirming the conjecture that including the 1% of the saturation mixing ratio over water threshold in the original RCEMIP protocol definition was, perhaps, too generously filling the domain with clouds. This is consistent with corresponding OLR images indicating that the domain does *not* fill with radiatively-active clouds, see Figures 2–5 of (Wing et al., 2020).

Second, the average increase in anvil temperature across the 10 K SST range for all models and for both domains (discussed further below) is substantially smaller for cfv2 (2.7 K) than for cfv0 (4.4 K, Wing et al., 2020)

STAUFFER AND WING 6 of 23



or cfv1 (4.5 K), indicating closer adherence to FAT/PHAT. This occurs because, when the saturation mixing ratio-component of the cloud condensate threshold is removed (cfv2, Figure 2), the profiles generally become smoother than those using cfv1 (Figure S1 in Supporting Information S1) and contain a clear and easily identified anvil peak using the upper-level peak in cloud fraction.

Wing et al. (2020) found that, with warming SST, anvil clouds rise robustly, slightly increase in temperature, and, for the majority of models, decrease in coverage. Anvil coverage is also reduced in simulations with aggregated convection (RCE_large) compared to those without aggregation (RCE_small). Although these results are unchanged when using a better calculation of cloud fraction applied consistently across all of the models (cfvl, see Text S1 in Supporting Information S1, cfv2, briefly reviewed below), cfv2 will be the definition we use and recommend since it is consistently applied across the models with explicit convection (unlike cfv0 of Wing et al., 2020) and because it is hypothesized to be a better representation indication of cloud fraction than cfv1.

With warming SST, the height of the anvil using cfv2 increases across all models for both RCE_small and RCE_large (Figures 3a and 3d). 79% of RCE_large simulations (Figure 3e) have an anvil that increases in temperature with warming SST (88% of models with explicit convection and 71% of models with parameterized convection, Figures S2b and S2e in Supporting Information S1). The average increase in anvil temperature (for those that increase) is larger from 300 to 305 K than 295–300 K. 82% of RCE_small simulations (Figure 3b) have an anvil that warms (86% of models with explicit convection and 73% of models with parameterized convection, Figures S1b and S1e in Supporting Information S1).

As for cloud fraction, two-thirds of RCE_large simulations have an anvil cloud fraction that decreases with warming SST where a larger percentage of the models with parameterized convection do so than those with explicit convection (70% and 63%, respectively, Figures S2c and S2f in Supporting Information S1). As in Wing et al. (2020), the trend in anvil cloud fraction for RCE_small is less pronounced than that in RCE_large. Approximately 58% of RCE_small exhibit a decrease in anvil cloud fraction with SST. Three of the models with explicit convection have zero overall change due to cloud fraction being near equal at 295 and 305 K and only slightly changing at 300 K (less than 1% change, Figure S1c in Supporting Information S1). If these are included in the percentage of models that do not have an increase in anvil coverage, 67% of RCE_small have a decrease in anvil coverage.

Why does cloud fraction increase with warming in a minority of models? This response cannot be completely attributed to the use of parameterized or explicit convection, nor can it be completely attributed to domain size. We tested the idea that cloud fraction has an absolute minimum, such that once it reaches that minimum it cannot decrease further. Unfortunately, there is no evidence that this is occurring in RCEMIP. For RCE_large, there are models with an increase in cloud fraction that have both small and large values of cloud fraction. There is also an equal number of models that have a decrease in cloud fraction for small and large values of cloud fraction. The same occurs for RCE_small. We note that, in general, models with explicit convection favor lower anvil coverage while models with parameterized convection favor higher anvil coverage, though the output of a cloud scheme may not be directly comparable to the threshold-based metric used for models with explicit convection.

Observational studies have found similar responses of anvil clouds to warming. For example, Igel et al. (2014) developed a cloud partitioning algorithm using CloudSat data and found that, with warming, cloud anvils rise and decrease in coverage (also found in Zelinka & Hartmann, 2011). Unlike our results, Igel et al. (2014) found cloud tops decreased in temperature with warming (a result also found using other methods, e.g., Singh & O'Gorman, 2012), however, as also argued by Holloway et al. (2017), the methods for analyzing observations versus using idealized equilibrium scenarios introduce inherent biases. Some of the issues noted by Igel et al. (2014) include the inability to completely isolate deep convecting clouds from other clouds in observational data set, limitations by resolution such as the integration of reanalysis data into their work, and limitations in the ability to isolate clouds from the influence of large-scale vertical motion. Conversely, Zelinka and Hartmann (2011), also using satellite data, found the temperature of high clouds to slightly warm (following PHAT more than FAT) with warming SST.

We also note that other factors besides SST play a role in driving changes in clouds (e.g., large-scale circulations; Lau et al., 1994; Wu & Moncrieff, 1999), but the idealization of RCE is designed to isolate the response of clouds to SST-forced climate warming. Therefore, in the next section, we test the Bony et al. (2016) stability-iris

STAUFFER AND WING 7 of 23



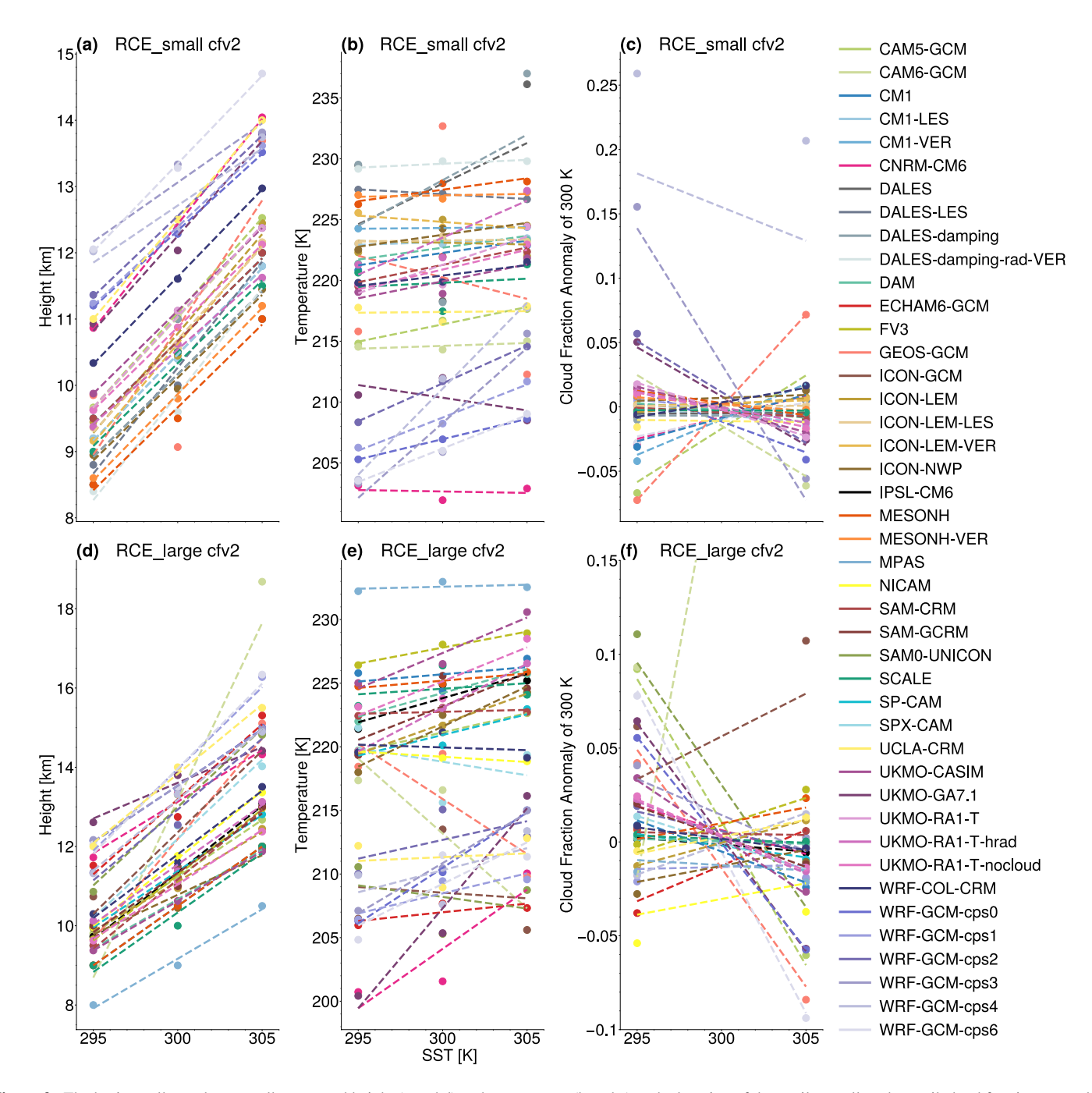


Figure 3. The horizontally- and temporally-averaged height (a and d) and temperature (b and e) at the location of the anvil as well as the anvil cloud fraction anomaly from 300 K (c and f) using the cfv2 definition. The top row (a, b, and c) is for the RCE_small simulations and the bottom row (d, e, and f) is for the RCE_large simulations. The linear regression line for a simulation is represented by the dashed lines. Note: in panel (f), the 305 K point for CAM6-GCM is off the chart.

hypothesis for a thermodynamic control on anvil cloud amount across the RCEMIP models and assess whether any further insight can be obtained on why some models have increasing anvil coverage with warming SST.

4. Controls on the Anvil Cloud Fraction

4.1. Testing the Stability Iris Theory

All RCE_large models (which have data available to calculate R_D and cfv2) have a R_D that decreases with increasing SST (Figure 4c). R_D decreases at an average rate of -0.022 days⁻¹ K⁻¹, although it ranges from -0.003

STAUFFER AND WING 8 of 23

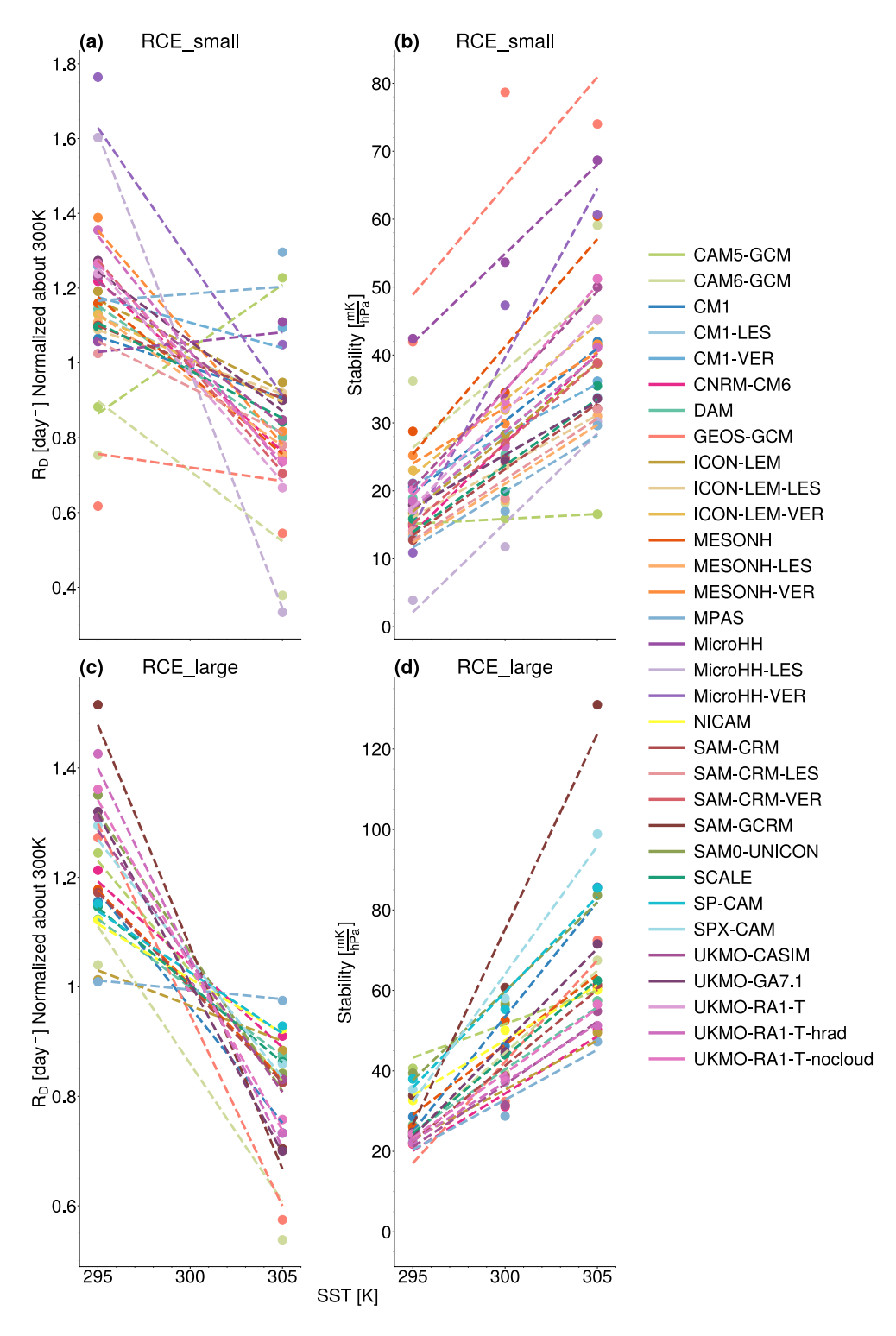


Figure 4. The horizontally- and temporally-averaged upper-level maximum of radiatively-driven divergence (a and c) and the static stability (b and d) at the location of the peak in radiatively-driven divergence. The top row (a and b) is for the RCE_small simulations and the bottom row (c and d) is for the RCE_large simulations. The linear regression line for a simulation is represented by the dashed lines.

STAUFFER AND WING 9 of 23



to -0.045 days⁻¹ K⁻¹. If R_D controls anvil cloud fraction, we would anticipate the location of the peak R_D to coincide with the anvil peak and, therefore, the slope of the heights of the anvil versus the height of R_D is equal to one. As seen in Figures 5a and 6a, this is approximately what occurs across all the models for both RCE_small and RCE_large, respectively. The height of the anvil tends to be lower than the height of peak R_D by $\sim 1.0-1.5$ km (not shown), but the heights vary together following close to a 1-to-1 ratio.

Figures 5b and 6b plot anvil cloud fraction against R_D where the hypothesis discussed above predicts that the 295 K simulations will be in the upper right quadrant (high values of both anvil cloud fraction and R_D) and the 305 K simulations will be in the lower left quadrant (low values of anvil cloud fraction and R_D). For RCE_large, cloud fraction and R_D decrease together for 80% of the models (note, this percentage is higher than the percentage of all models with a decrease in cloud fraction discussed in Section 3 because here we consider the smaller population of models for whom the data to calculate R_D is available). When Q_r is held constant at its 300 K value, R_{D300Q} and anvil cloud fraction in RCE_large once again decrease together with warming (Figure 6c). However, when stability is held constant at its 300 K value, cloud fraction and R_{300S} are negatively correlated in all but 25% of RCE_large models (Figure 6d). In the 25% with an apparent positive correlation, cloud fraction and R_{D300S} increase together with warming SST in all but one of those models. Across the suite, R_{D300S} increases with warming SST when stability is held constant, the opposite response as the full calculation (R_D). This tells us that stability changes are responsible for R_D decreasing with warming SST and, thus, anvil cloud fraction decreas-

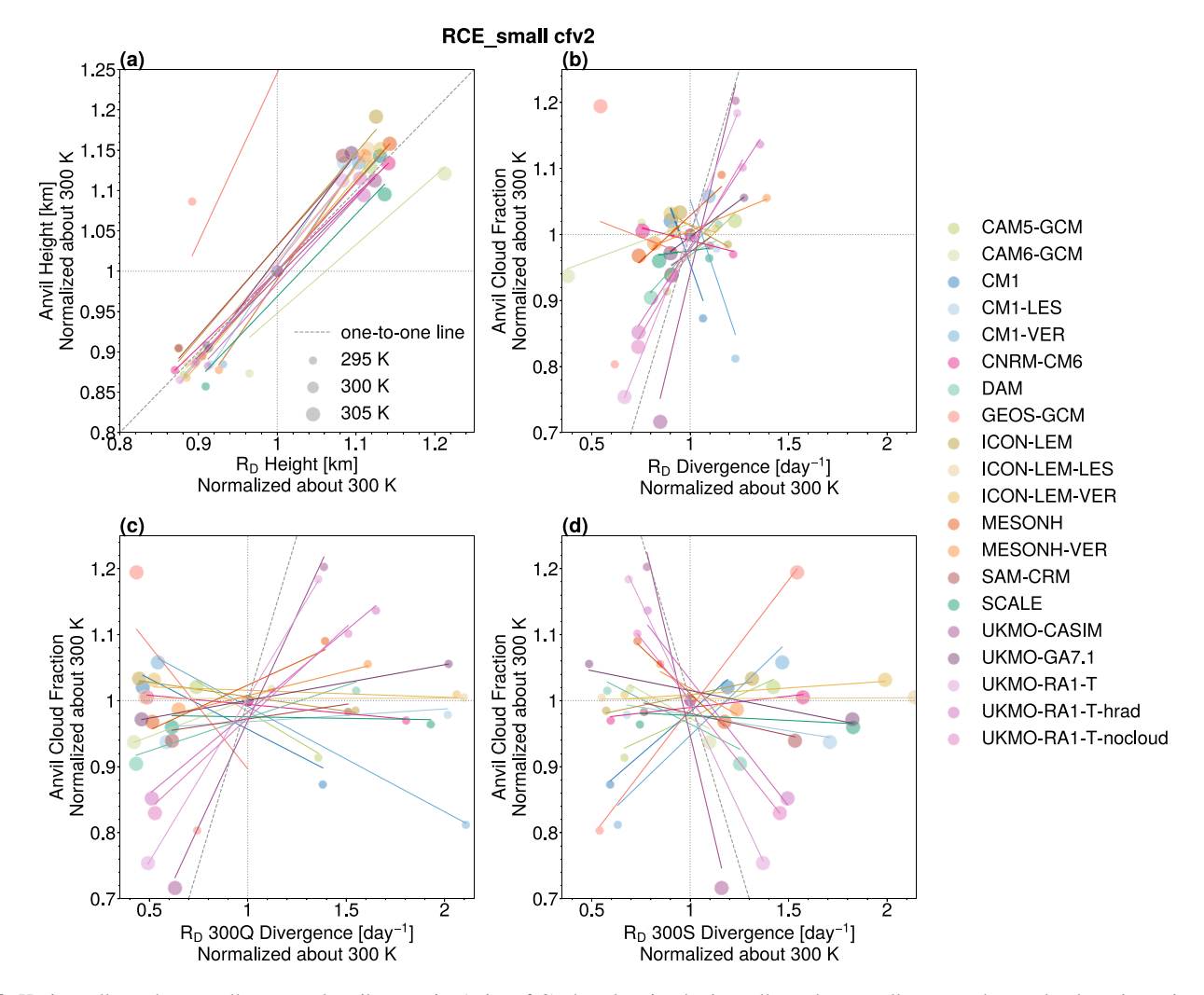


Figure 5. Horizontally- and temporally-averaged anvil properties (using cfv2) plotted against horizontally- and temporally-averaged upper-level maximum in radiatively-driven divergence (R_D) properties for RCE_small. (a) Plots the heights of the anvil against the height of R_D while the remaining panels (b) plot the anvil cloud fraction against R_D for the "full" calculation of R_D , (c) R_D with the radiative cooling rate held fixed at 300 K, and (d) R_D with static stability held fixed at 300 K. The solid lines depict the linear regression line. All values for all panels are normalized about their value at 300 K.

STAUFFER AND WING 10 of 23



ing with SST. This is because, when variability in stability is removed by holding it constant, the correlation between cloud fraction and R_D changes, while it does not when removing variability in the radiative cooling rate.

The RCE_small simulations behave less consistently than the RCE_large simulations. 89% of the RCE_small simulations exhibit a decrease in R_D with SST (Figure 4a) but only 65% show cloud fraction and R_D decreasing together (Figure 5b). Although the behavior is less robust for RCE_small, anvil cloud fraction and R_{D300Q} (Q_r is held constant at 300 K) still decrease together (in 60% of models, Figure 5c) and anvil cloud fraction and R_{D300S} (stability is held constant at 300 K) are negatively correlated for all but 25% of the models (Figure 5d), like RCE_large.

4.2. Explaining Inconsistencies in the Stability Iris Theory

The positive correlation between R_D and cloud fraction holds for many, but not all the models and does not explain the inter-model spread in cloud fraction for a given SST. This inconsistency is not easily explained but it is a consequence of cloud fraction, alone, not always decreasing with warming across the models. For RCE_large, four models (of those which have data for the cfv2 and R_D calculations) have an anvil cloud fraction which increases with warming despite a decrease in R_D : three with explicit convection schemes (including one

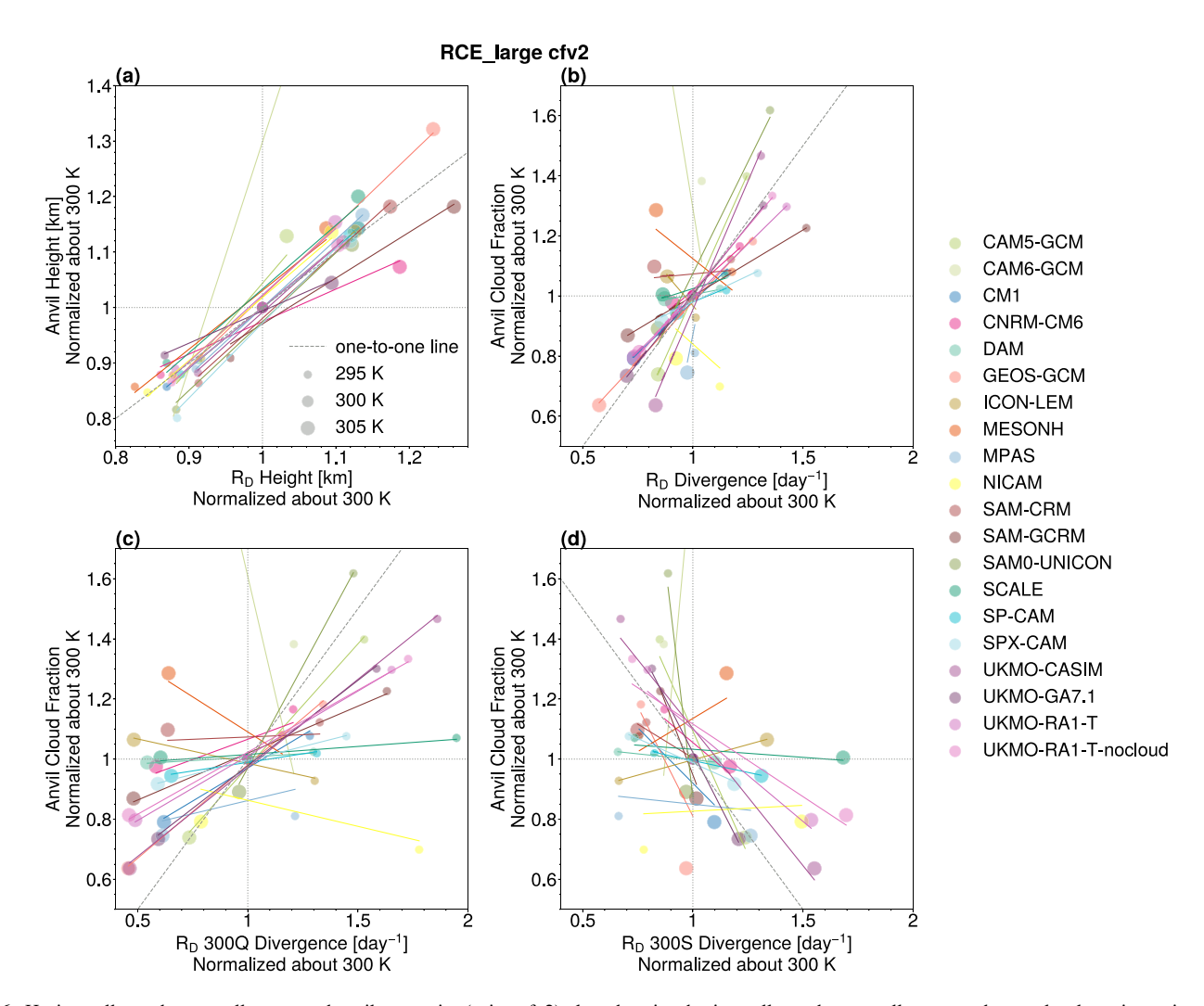


Figure 6. Horizontally- and temporally-averaged anvil properties (using cfv2) plotted against horizontally- and temporally-averaged upper-level maximum in radiatively-driven divergence (R_D) properties for RCE_large. (a) Plots the heights of the anvil against the height of R_D while the remaining panels (b) plot the anvil cloud fraction against R_D for the "full" calculation of R_D , (c) R_D with the radiative cooling rate held fixed at 300 K, and (d) R_D with static stability held fixed at 300 K. The solid lines depict the linear regression line. All values for all panels are normalized about their value at 300 K.

STAUFFER AND WING 11 of 23



GCRM) and one with parameterized convection, CAM6-GCM. The domain-filled cloud coverage at 305 K in CAM6-GCM is known to be spurious (Reed et al., 2021), so we discard its behavior.

For RCE_small, seven models have increasing cloud fraction with warming despite a decrease in R_D . Five of these models have explicit convection which come from two families; CM1 and its VERT companion and ICON-LEM and its VERT and LES companions. The two models with parameterized convection that have this behavior represent 40% of the RCE_small models with parameterized convection which have the appropriate data for the RCE_small R_D calculation.

Although the majority of models for which the divergence hypothesis does not hold due to a negative correlation between R_D and cloud fraction are those with explicit convection schemes (across both RCE_small and RCE_large), the breakdown cannot be completely attributed to models using explicit convection, as it also occurs in some of the models with parameterized convection. Inconsistencies within the models with parameterized convection occur only in their RCE_small SCM simulations (with the exception of the spurious RCE_large CAM6-GCM). This may suggest that this is less an issue occurring within models with parameterized convection and rather issues with using single-column models, rather than using a population of columns, to represent the RCE state. Similarly, it is notable that the models with explicit convection that have the negative R_D -cloud fraction correlation happen to also be models with VERT and LES counterparts, but this doesn't necessarily mean VERT and LES simulations stand out as having increases in cloud fraction because the whole sample of VERT and LES simulations are not represented by this response and the response does not completely exclude standard CRM simulations.

There is one additional model in RCE_small that behaves differently. The CAM5-GCM single column model has a positive correlation between R_D and cloud fraction, but that is because the two properties *increase* as opposed to decrease together with warming SST. Thus, the radiatively-driven divergence still explains the cloud behavior, just not in the manner expected. Otherwise, increases in cloud fraction with warming are *not* explained by the R_D theory. Of the 12 models that have an increase in cloud fraction with warming SST (across domains), only this single model is accompanied by an increase in R_D .

Similar to R_D , removing variability in static stability and the radiative cooling rate (separately) does not explain the increasing anvil cloud fraction occurring in some models. When variability in the radiative cooling rate is removed, all models have R_D decreasing with warming SST and, similarly, when variability in static stability is removed, all models have R_D increasing with warming SST (except for SAM-CRM RCE_large, where R_D and cloud fraction both decrease with warming SST).

An additional factor that may modulate the R_D -cloud fraction relationship is changes in aggregation with warming. Aggregation is known to decrease high cloud fraction compared to un-aggregated simulations (Wing et al., 2020). Many models, but not all, have an increase in aggregation with warming and a decrease in cloud fraction, or, a decrease in aggregation with warming and an increase in cloud fraction (top left and bottom right quadrants of Figure 7, respectively). Changes in aggregation could therefore potentially explain failures of the R_D theory (anvil peak cloud fraction increasing despite R_D decreasing). Many cases of aggregation decreasing with warming are associated with such a failure (the cluster of red markers in the bottom right quadrant of Figure 7). Decreases in aggregation with warming may thus be what pushes the cloud fraction of the anvil to increase despite the decrease in R_D . However, this does not hold true for all cases; there are plenty of cases where the R_D theory holds despite decreases in aggregation (green markers in the bottom left quadrant of Figure 7). The reduction in anvil cloud fraction with aggregation has been explained in terms of the decrease in R_D that results from a warmer atmosphere with aggregation (Bony et al., 2016), so it is also unclear how changes in R_D could control the anvil cloud fraction response to changes in aggregation but not the response of anvil cloud fraction to changes in SST in the same manner.

This leads us to propose that R_D is not the sole control of cloud fraction, that perhaps other processes play important roles in addition to radiative cooling. For example, recent work has addressed the topic by studying the lifetime of an anvil cloud (which is affected by microphysics and the timescales of ice vs. liquid water), studying effects of evaporative cooling in addition to radiative cooling, and studying sensitivities to the vertical resolution of models (Beydoun et al., 2021; Jeevanjee & Zhou, 2022; Ohno & Satoh, 2018; Ohno et al., 2019, 2020, 2021; Seeley, Jeevanjee, Langhans, & Romps, 2019; Seeley, Jeevanjee, & Romps, 2019). Additionally, R_D has to be interpreted carefully as it represents net detrainment (which can be negative) rather than gross detrainment (which

STAUFFER AND WING 12 of 23

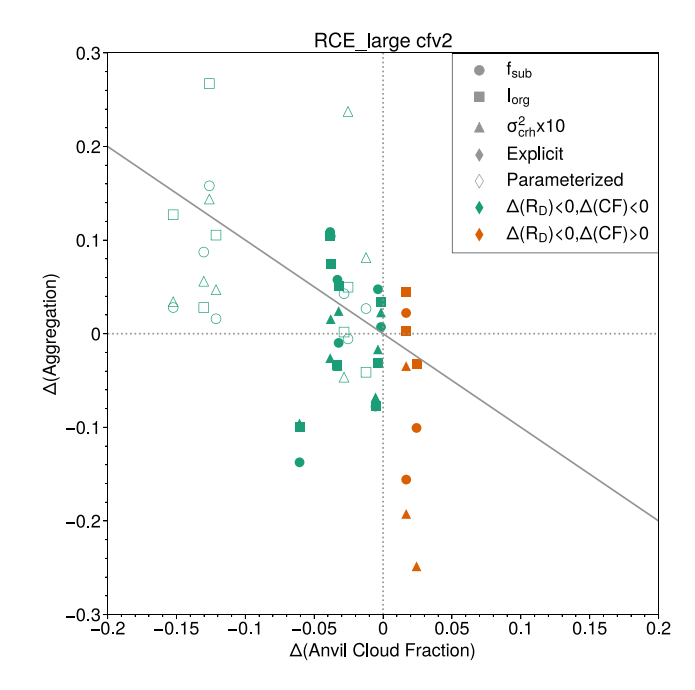


Figure 7. Changes in aggregation with warming using three metrics (subsidence fraction, index of organization, and the variance in column relative humidity, represented by the different marker shapes) versus changes in anvil cloud fraction with warming using cfv2 for the RCE_large simulations. The models with explicit convection are the solid markers while the models with parameterized convection are the open markers. Aggregation data is from Wing et al. (2020). Note: CAM6-GCM is off the chart due to its large increase in cloud fraction. All combinations of changes in R_D versus changes in cloud fraction are captured by the green and red markers, which represents whether the stability iris theory succeeds (green) or fails (red).

is nonnegative) resulting in the ability of the metric to change signs between the upper and lower atmosphere unlike cloud fraction which is only positive (Jeevanjee & Zhou, 2022; Seeley, Jeevanjee, & Romps, 2019). That said, the simulations in RCEMIP provide strong support for R_D as a leading order control of changes in anvil cloud fraction with warming.

5. Controls on the Mid-Level Cloud Fraction

Mid-level clouds robustly decrease with warming SST across the models (Figures 8 and 9a solid markers), consistent with Cronin and Wing (2017). The simulations at different SST also robustly collapse to a single profile when plotted against temperature, compare the solid (temperature-space) lines to the dashed (height-space) lines in Figure 8. This can also be seen in Figure 9d where the range, calculated using Equation 4, of mid-level cloud fraction is smaller in temperature space (solid triangles) than in height space (solid circles). The models with parameterized convection have a much greater decrease in mid-level clouds with warming SST than models with explicit convection (compare the solid circles on the right to those on the left in Figure 9d) but still collapse to a comparable range in temperature space (solid triangles in Figure 9d). The average difference between $\langle CF_{\rm range} \rangle$ in height space and $\langle CF_{\rm range} \rangle$ in temperature space is 0.06 across the model suite, where the models with parameterized convection have a larger difference at 0.08 than the models with explicit convection at 0.03. In fact, the average difference between $\langle CF_{\rm range} \rangle$ in temperature space and $\langle CF_{\rm range} \rangle$ in height space is 82% of their $\langle CF_{\rm avg}^{-} \rangle$ value (88% for models with parameterized convection and 74% for models with explicit convection), which tells us the range in temperature space is smaller than the magnitude of the cloud fraction value itself and therefore the mid-level cloud fraction roughly collapses to one profile when plotted in temperature space across the models.

Because the behavior of mid-level clouds is similar for both models with explicit convection and models with parameterized convection (despite the

noted lack of mid-level clouds in GCMs, Boucher et al., 2014; Randall et al., 2007; Zhang, 2005), the style of convection cannot completely explain differences in mid-level cloud behavior. Further analysis of the mid-level clouds, at least in the manner we use for the models with explicit convection, cannot be completed with the GCMs due to the inability to compute statistics conditionally averaged over convecting/cloudy areas from offline, coarse GCM output. Thus, the rest of this section focuses on the models with explicit convection.

The mid-level scaling diagnostic of Cronin and Wing (2017) (Section 2.4.2; Equation 5) applied to the models with explicit convection (open markers of Figures 9a and 9d) captures the decrease in mid-level clouds and their collapse in temperature space. This is shown by the negative values of $\langle \Delta CF \rangle$ as predicted by the diagnostic scaling in Figure 9a (open markers) as well as the cloud fraction range as predicted by the diagnostic scaling being larger in height space than temperature space (open circles are above open triangles in Figure 9d). The difference in cloud fraction as predicted by the scaling diagnostic compared to the difference in mid-level cloud fraction of cfv2 lie approximately on a 1-to-1 line with reasonably high correlations (Figure 9b) for both height space (circles) and temperature space (triangles). The commonality in the behavior of the cfv2 cloud fraction profiles and the cloud fraction profile predicted by the mid-level scaling diagnostic allows us to take advantage of the diagnostic scaling (Equation 5) to analyze how its components change with respect to each other with warming and determine a control on the mid-level clouds with reasonable physical backing.

All the terms of Equation 5 also collapse in temperature space for most models. For example, Figures 10 and 11 display profiles of integrated radiative cooling and environmental relative humidity, respectively, plotted in both height-space (dotted lines) and temperature-space (solid lines). The invariance in these variables was also found by Cronin and Wing (2017), but here we verify the robustness of these invariances across a wide range of models. While there are not sound physical explanations for the collapse of

STAUFFER AND WING 13 of 23



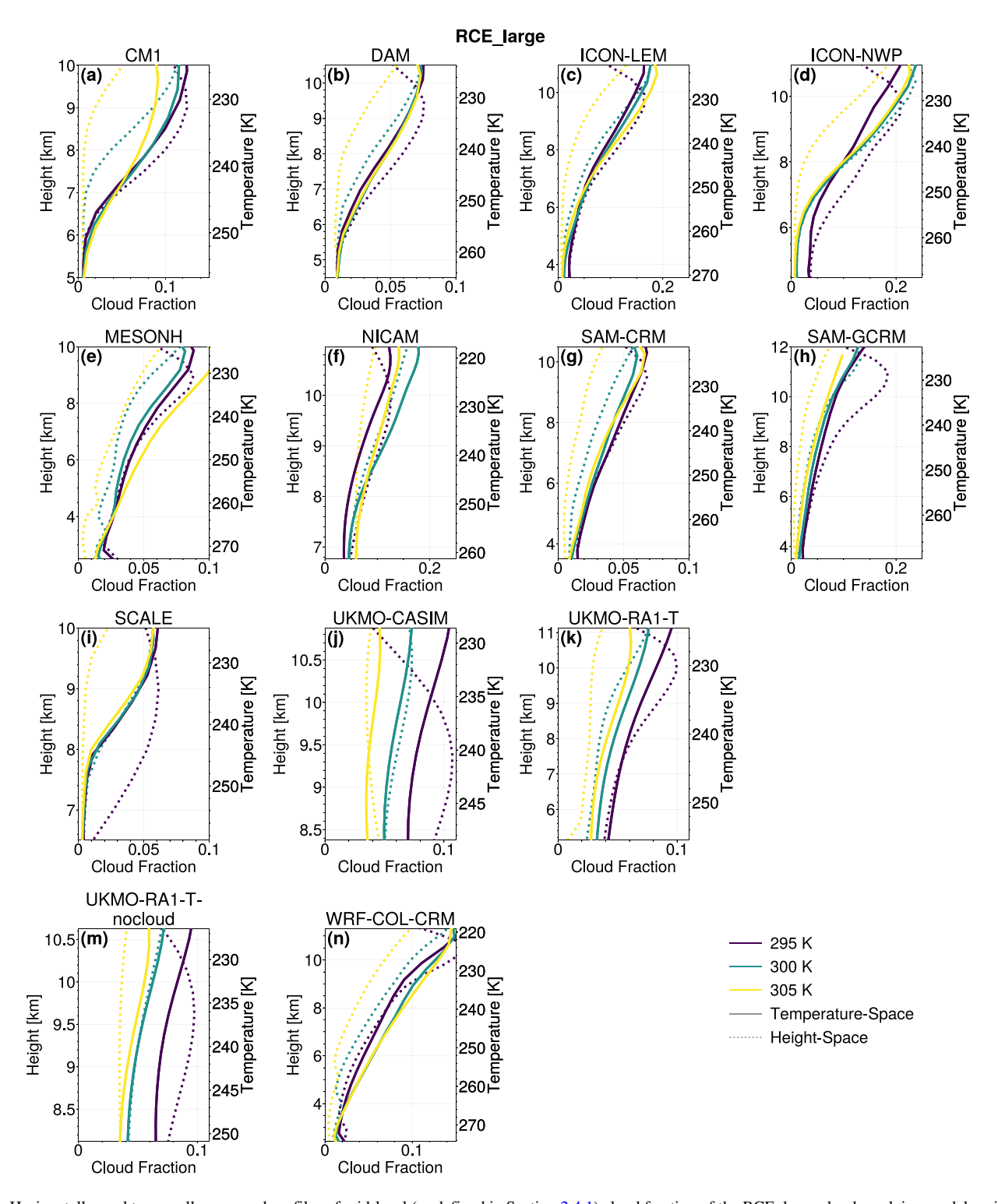


Figure 8. Horizontally- and temporally-averaged profiles of mid-level (as defined in Section 2.4.1) cloud fraction of the RCE_large cloud resolving models using cfv2, plotted against height space (dotted lines, left axis) and temperature (solid lines, right axis) for 295, 300, and 305 K (purple, green, and yellow lines, respectively). Note: the ranges of the vertical axes vary since the mid-level range are model-dependent.

some of the terms, the invariance of relative humidity and radiative cooling to changing temperatures have an established physical basis and significant implications for other aspects of climate (Figures 9e and 9f; Ingram, 2010; Jeevanjee & Romps, 2018; Po-Chedley et al., 2019; Romps, 2014). Romps (2014) used basic

STAUFFER AND WING 14 of 23



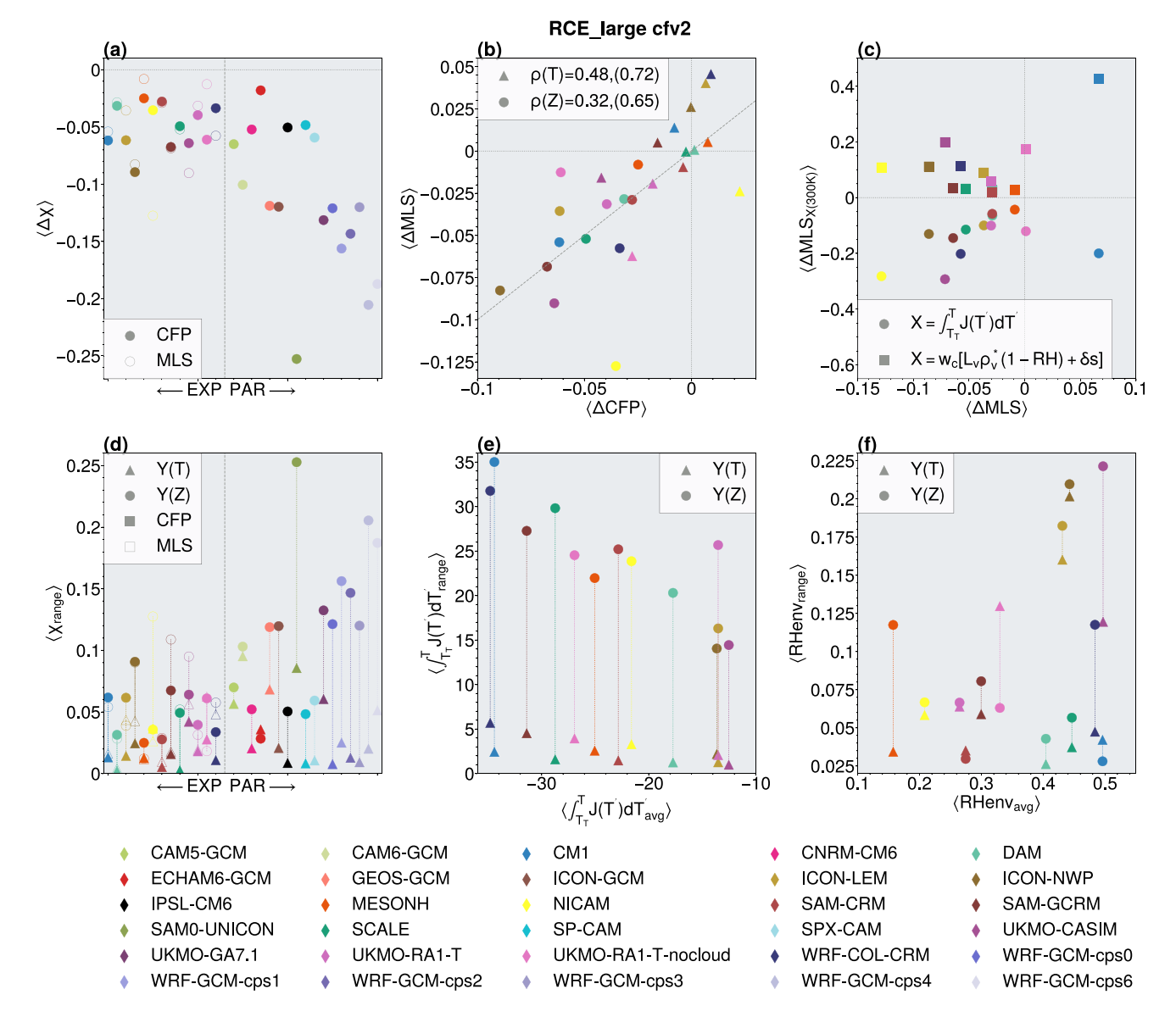


Figure 9. Scatter plots of the mid-level clouds using the mid-level scaling metrics defined in Section 2.4.1. (a) Plots the difference between 305 and 295 K cloud fraction profiles (closed markers; CFP) and for the mid-level diagnostic defined in Section 2.4.2 (open markers; MLS). (b) Depicts the correlation of the change in MLS and CFP plotted in temperature space (triangles) and height space (circles). The correlations out of the parentheses are representative of all of the models while the correlations in parentheses exclude the outlier, NICAM (yellow points). (c) Plots the change in MLS (Equation 5) with sea surface temperature if the numerator and denominator are individually held constant at their 300 K value against ⟨Δ*MLS*⟩. (d) Plots the range of CFP (closed markers) and MLS (open markers) in both height space (circles) and temperature space (triangles). (e and f) Plot the range of the tropospheric radiative cooling rate and the range in environmental relative humidity (respectively) in both height space (circles) and temperature space (triangles) against their average value in temperature space. Notes: (a) The *x*-axes in panels (a and d) mean nothing, models with parameterized convection are on the right side of the vertical gray line and models with explicit convection are on the left side of the vertical gray line. (b) (b, c, e, and f) show only the models with explicit convection. (c) (d, e, and f) have lines that connect the metric in height space to the metric in temperature space for visual aid.

and well-understood physics to derive an equation governing the invariant nature of the "RH-T curve" with conclusions similar to FAT: the profile shifts upward (also seen in Po-Chedley et al., 2019) in order to maintain the same temperature. This stemmed from Romps (2014) noting the consistent shape and range of relative humidity profiles in all manners of data (observations, GCMs, and CRMs). Po-Chedley et al. (2019) found that the intermodel spread in CMIP models in response to CO₂-forced warming can be explained by the upward shift in cloud fraction and relative humidity fields to maintain a constant temperature-space profile. Similarly, Jeevanjee and Romps (2018) discuss the invariance of radiative cooling, which is found in RCE as well as comprehensive GCMs, which has implications for constraints on precipitation in a warm-

STAUFFER AND WING 15 of 23



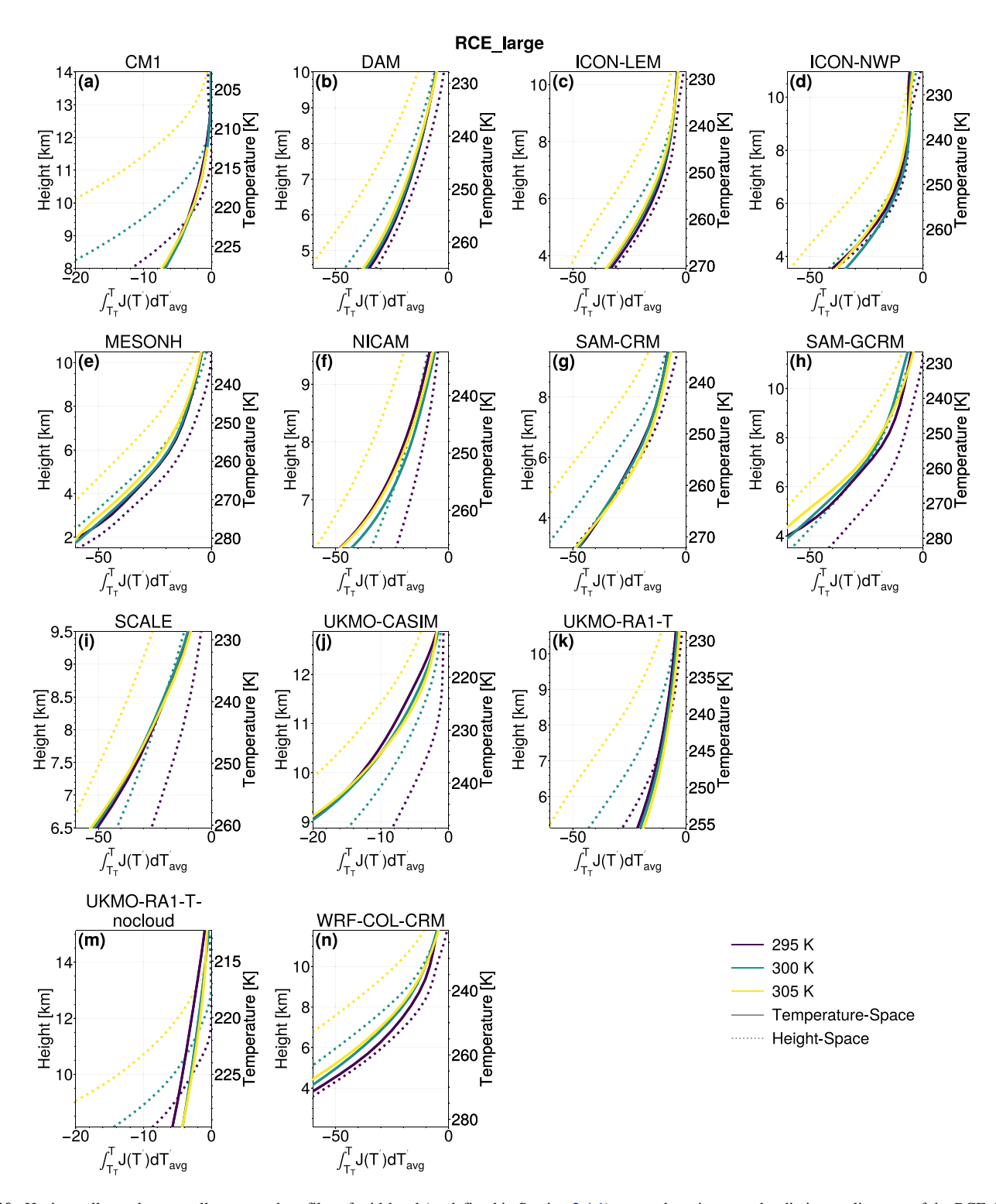


Figure 10. Horizontally- and temporally-averaged profiles of mid-level (as defined in Section 2.4.1) troposphere-integrated radiative cooling rate of the RCE_large cloud resolving models using cfv2, plotted against height space (dotted lines, left axis) and temperature (solid lines, right axis) for 295, 300, and 305 K (purple, green, and yellow lines, respectively). Note: the ranges of the vertical axes vary since the mid-level range are model-dependent.

ing climate. We do note that for relative humidity (Figures 9f and 11) there is generally greater scatter and less consistency as three models have the opposite behavior: the metric in temperature space has a greater range than the metric in height space. Finally, the radiative cooling in general collapses better in temperature

STAUFFER AND WING 16 of 23



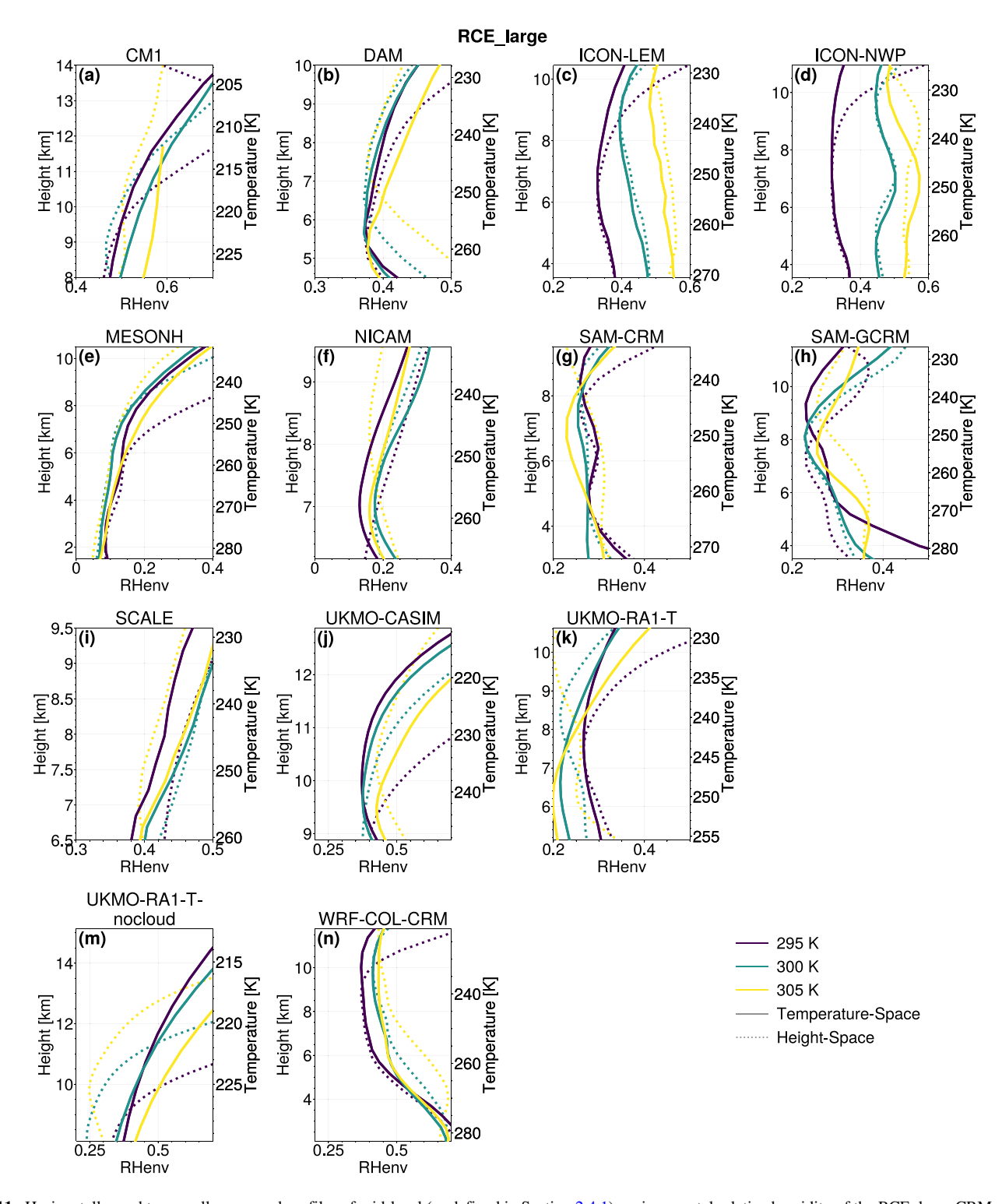


Figure 11. Horizontally- and temporally-averaged profiles of mid-level (as defined in Section 2.4.1) environmental relative humidity of the RCE_large CRMs using cfv2, plotted against height space (dotted lines, left axis) and temperature (solid lines, right axis) for 295, 300, and 305 K (purple, green, and yellow lines, respectively). Note: the ranges of the vertical axes vary since the mid-level range are model-dependent.

STAUFFER AND WING 17 of 23



space than relative humidity does, considering the range in temperature space relative to the average values. This seems obvious when looking at the profiles in Figure 10 or 11 or the distance between the circle and triangle scatters in Figures 9e and 9f, but, to account for the difference in order of magnitude between the two terms, the conclusion was verified by comparing the term-relative ratio of the ranges in height and temperature space to their corresponding average in temperature space (i.e., the *y*-axis divided by the *x*-axis of Figure 9, not shown).

Cronin and Wing (2017) discussed that the mid-level cloud fraction decreases because the denominator of Equation 5, the product of cloud updraft speed and cloud vapor density excess, increases with warming much faster than the numerator of Equation 5, the tropospheric radiative cooling rate. This holds true across the RCEMIP ensemble where Figure 9c shows that, when the numerator is held constant at its 300 K value (circles of Figure 9c), the mid-level cloud fraction (as predicted by the diagnostic scaling) decreases ($\langle \Delta MLS \rangle$ is negative) as expected but, when the denominator is held constant at its 300 K value (squares of Figure 9c), the mid-level cloud fraction (as predicted by the diagnostic scaling) increases ($\langle \Delta MLS \rangle$ is positive). If it were up to the numerator, mid-level clouds would increase. That they decrease instead indicates that the increase in the denominator overwhelms the increase in the numerator.

In summary, the diagnostic scaling for mid-level clouds captures (a) a decrease in mid-level cloud fraction with warming, (b) a collapse of cloud fraction to one profile in temperature space, and (c) the value of mid-level cloud fraction.

We note that the profiles of cloud fraction on a temperature axis look very similar to shifting the profile upwards in height with warming SST, to align the anvil peaks (not shown). The collapse of the profiles when shifted upward is consistent with the collapse in temperature space (and thus, explanation by the mid-level scaling) because the location of the anvil peak is constrained by temperature. That is, the profiles move upward in order to remain at the same temperature.

6. Conclusion and Discussion

The wide range of models within the RCEMIP data set provides a unique opportunity to investigate the fundamental properties of deep convection and determine which behaviors emerge as robust across models despite their different representations of numerics, physics, etc. In particular, we are able to compare the controls on deep convecting clouds in models that represent such clouds explicitly versus those that parameterize them. Future work should explore whether these properties and controls manifest themselves robustly in observations of the tropical atmosphere. Using this diverse set of models, this paper verified and solidified hypotheses from prior literature and presented an analysis of anvil cloud properties in a similar manner to Wing et al. (2020) using a consistently applied definition of cloud fraction. Our results agree that the height of anvil clouds increases robustly, the temperature of the anvils increase slightly for the majority of the models following the PHAT hypothesis (Zelinka & Hartmann, 2010), and the anvil cloud amount decreases for two-thirds of the models with warming SST.

We then tested the stability iris theory (Bony et al., 2016; Zelinka & Hartmann, 2010) on the control of high cloud fraction. The theory holds for those models which have a decrease in cloud fraction with warming SST. However, there are some models that have an increase in anvil cloud fraction despite a decrease in R_D . Although we considered several possible explanations, we are left speculating that perhaps radiatively-driven divergence cannot completely explain how anvil cloud fraction changes with warming. Nevertheless, the high correlation between changes in R_D and cloud fraction leads us to conclude that R_D plays a leading role in the control of anvil coverage. This is consistent with the conclusions of Beydoun et al. (2021), which argues that the need to account for detrainment and lifetime of ice in definition of an anvil doesn't mean that radiatively-driven divergence cannot explain cloud fraction responses to warming temperature (as argued in Seeley, Jeevanjee, Langhans, & Romps, 2019; Seeley, Jeevanjee, & Romps, 2019), rather, that radiatively-driven divergence is simply a determining factor of anvil cloud fraction.

We also found that the mid-level clouds decrease with SST across all the models and also tend to collapse to a common profile when plotted in temperature space. These results are captured by a scaling diagnostic for the mid-level clouds developed by Cronin and Wing (2017). All terms of the diagnostic equation collapse to one

STAUFFER AND WING 18 of 23



profile when considered as a function of temperature, although some terms do so more strongly than others. Our results confirm the temperature invariance of relative humidity and radiative cooling profiles, which has important implications for other aspects of climate (Jeevanjee & Romps, 2018; Po-Chedley et al., 2019; Romps, 2014). We also find that the overall convective heating of clouds increases at a much faster rate than the integrated radiative cooling rate, causing the cloud fraction to decrease according to this diagnostic scaling.

Although there are many benefits presented by such a diverse group of models in the RCEMIP data set, there are difficulties in trying to compare results across the entire suite. First, the cloud fraction variable is itself an artificial construct. Clouds are not a binary object but rather a continuous transition from clear sky to optically and physically thick condensate. Consequently, a host of assumptions are made when defining a cloud in a subgrid-scale scheme or by considering a threshold value of cloud condensate. Both methods are individually flawed and imperfect in different ways, but it is also unclear whether the two approaches (used in models with parameterized convection and explicit convection, respectively) are directly and quantitatively comparable to each other. Furthermore, the limitations of the coarse grid and parameterization in GCMs prevents us from applying some of our analysis to those models, such as the ability to rigorously test different definitions for variables or compute statistics over cloud areas.

Despite these limitations, the RCEMIP data set provides a valuable opportunity to understand how clouds respond to a warming surface temperature. While the cloud fraction values may not be directly comparable between models with parameterized convection and explicit convection, the behavior of the clouds with warming is generally similar. To first order, the hypotheses controlling high and mid-level clouds hold in both the models with explicit and parameterized convection, which strengthens our conclusions.

We have used the RCEMIP simulations to describe what the deep-convective cloud response to warming is and why the clouds change the way that they do. Future work will take the next step by investigating how these cloud changes contribute to climate feedbacks. The tropical anvil cloud feedback is the largest source of uncertainty in climate sensitivity (Sherwood et al., 2020). The common framework of the RCEMIP data set may aid in determining what the tropical cloud feedback is, its decompositions into contributions from the longwave and shortwave, as well as the contributions from different types of clouds as defined by, for example, altitude and optical thickness. One of the few areas in which the RCEMIP models with explicit convection have closer agreement than the models with parameterized convection is in the change in cloud radiative effect with warming (Wing et al., 2020). This lends optimism that a proper calculation of cloud feedbacks (i.e., with radiative kernels or partial radiative perturbations) and their decomposition in the RCEMIP models with explicit convection (a task usually limited to models with parameterized convection) will help constrain the tropical anvil cloud feedback.

Appendix A: Using 3D Data to Calculate Cloud Fraction

The equilibrium state used in our analysis consists of time-averaged profiles, excluding the first 75 days of the simulation. Since cfv1 and cfv2 are domain-wide metrics computed from the 3D data, the time-average is derived from six-hourly instantaneous snapshots. cfv0, on the other hand, is derived from the domain- and hourly-averaged 1D profiles, which themselves are based on sampling at a much higher frequency (i.e., in SAM-CRM, every 8 minutes). The reduced sampling in cfv1 and cfv2 from using 3D data may introduce a bias. We test the validity of using the 3D data to recalculate time-averaged cloud fraction through its usage in SAM-CRM (Khairoutdinov & Randall, 2003). This model was run in-house and therefore the processes used to diagnose variables as well as sampling are completely known. This is especially important in comparing cfv0 and cfv1 where, for SAM-CRM, the definitions are identical and therefore differ only in the temporal sampling. We found that the temporally-averaged profiles of cfv0 and cfv1 agree with one another, including anvil height and amount, the crux of the analysis in this paper (Figure A1).

STAUFFER AND WING 19 of 23

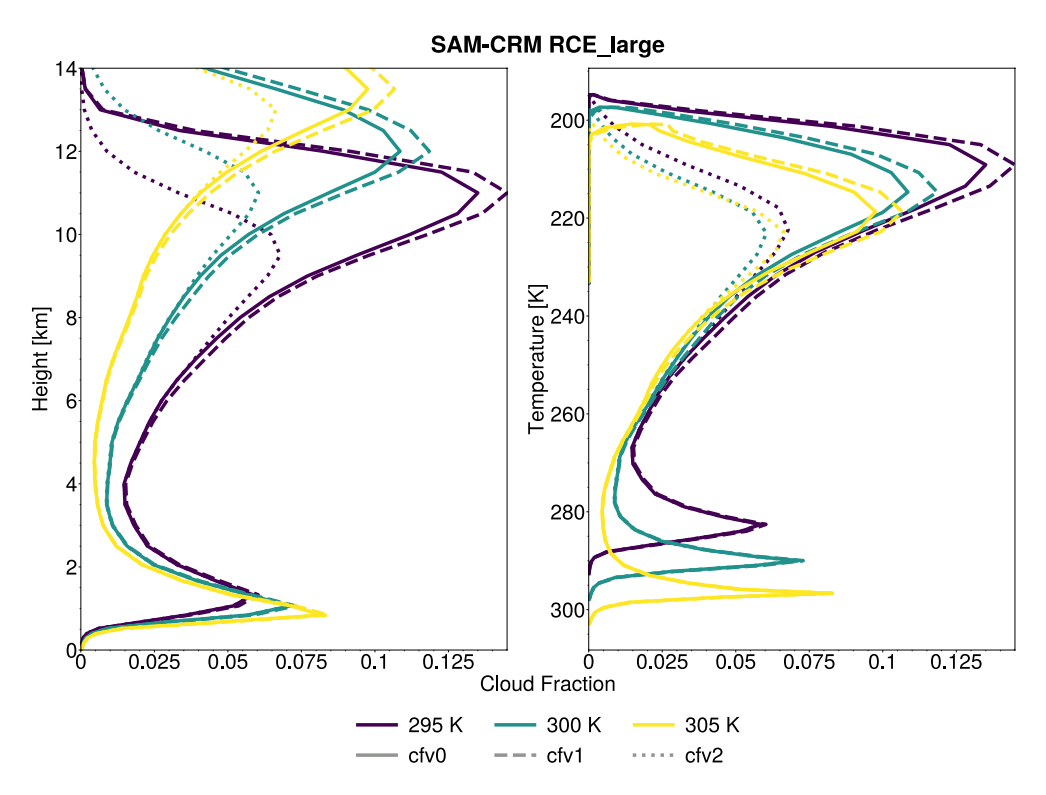


Figure A1. Horizontally- and temporally-averaged profiles of cloud fraction plotted against (a) height and (b) temperature for SAM-CRM RCE_large. The colored profiles, purple, green, and yellow, are the simulations at sea surface temperatures of 295, 300, and 305 K, respectively and the solid, dashed, and dotted lines represent the three definitions of cloud fraction, cfv0, cfv1, and cfv2, respectively.

Some models have a substantial difference between cfv0 and the 3D derived cloud fraction profiles (cfv1), even if the correct threshold was used for cfv0 (Figures S4 and S5 in Supporting Information S1). We speculate that any number of factors may be responsible for this discrepancy. Saturation mixing ratio, an integral part of the cfv0 and cfv1 definition, may have been calculated based on saturation over ice for cfv0 instead of water, a known non-negligible subtlety. The equation used could also differ across models. For all models, the calculation of the saturation vapor pressure for cfv1 applied the definition used in SAM-CRM which uses the eighth order polynomial fit to the Wexler (1976) expression for saturation vapor pressure developed by Flatau et al. (1992). Nevertheless, the remarkable consistency between profiles of cloud fraction for the cfv0 and cfv1 definitions in SAM-CRM (Figure A1) leads us to be confident in the use of the more limited sampling of the 3D model output to generate the time- and domain-mean profiles.

The consistently applied definition in cfv1 and cfv2 then allows for a fairer comparison of cloud properties across models. In Text S1 in Supporting Information S1, we repeat the analysis of Wing et al. (2020) (which used cfv0) using cfv1, to compare to the analysis of cfv2 presented in Section 3.

Data Availability Statement

We thank the German Climate Computing Center (DKRZ) for hosting the standardized Radiative Convective Equilibrium Model Intercomparison Project (RCEMIP) data, including the new versions of cloud fraction diagnosed here, which is publicly available at http://hdl.handle.net/21.14101/d4beee8e-6996-453e-bbd1-ff-53b6874c0e. Data derived from the RCEMIP data set are archived at https://doi.org/10.5281/zenodo.6323552 (Stauffer & Wing, 2022).

STAUFFER AND WING 20 of 23



Acknowledgments

We acknowledge support by NSF-AGS 1830724. We thank all co-authors on the Radiative Convective Equilibrium Model Intercomparison Project (RCEMIP) overview paper (Wing et al., 2020) for providing the RCEMIP simulations. We would also like to thank Dr. Nadir Jeevanjee and an anonymous reviewer for their constructive and thorough reviews. C. L. Stauffer wishes to thank her Ph.D. committee members: Drs. Alyssa Atwood, Eric Chicken, Mark Bourassa, and Guosheng Liu for their support and early feedback on this work.

References

- Abbott, T. H., Cronin, T. W., & Beucler, T. (2020). Convective dynamics and the response of precipitation extremes to warming in radiative—convective equilibrium. *Journal of the Atmospheric Sciences*, 77(5), 1637–1660. https://doi.org/10.1175/JAS-D-19-0197.1
- Becker, T., & Wing, A. A. (2020). Understanding the extreme spread in climate sensitivity within the radiative–convective equilibrium model intercomparison project. *Journal of Advances in Modeling Earth Systems*, 12(10), e2020MS002165. https://doi.org/10.1029/2020MS002165
- Beydoun, H., Caldwell, P. M., Hannah, W. M., & Donahue, A. S. (2021). Dissecting anvil cloud response to sea surface warming. *Geophysical Research Letters*, 48(15), e2021GL094049. https://doi.org/10.1029/2021GL094049
- Blossey, P. N., Bretherton, C. S., & Wyant, M. C. (2009). Subtropical low cloud response to a warmer climate in a superparameterized climate model. Part II: Column modeling with a cloud resolving model. *Journal of Advances in Modeling Earth Systems*, 1(3), 8. https://doi.org/10.3894/JAMES.2009.1.8
- Bony, S., Colman, R., Kattsov, V. M., Allan, R. P., Bretherton, C. S., Dufresne, J.-L., et al. (2006). How well do we understand and evaluate climate change feedback processes? *Journal of Climate*, 19(15), 3445–3482. https://doi.org/10.1175/JCLI3819.1
- Bony, S., Stevens, B., Coppin, D., Becker, T., Reed, K. A., Voigt, A., & Medeiros, B. (2016). Thermodynamic control of anvil cloud amount. Proceedings of the National Academy of Sciences, 113(32), 8927–8932. https://doi.org/10.1073/pnas.1601472113
- Bony, S., Stevens, B., Frierson, D. M. W., Jakob, C., Kageyama, M., Pincus, R., et al. (2015). Clouds, circulation and climate sensitivity. *Nature Geoscience*, 8(4), 261–268. https://doi.org/10.1038/ngeo2398
- Boucher, O., Randall, D., Artaxo, P., Bretherton, C., Feingold, G., Forster, P., et al. (2014). Clouds and aerosols. In T. F. Stocker, D. Qin, G.-K. Plattner, M. Tignor, S. K. Allen, J. Boschung, et al. (Eds.), Climate change 2013: The physical science basis. Contribution of working group I to the fifth assessment report of the intergovernmental panel on climate change (pp. 571–658). Cambridge University Press.
- Bretherton, C. S. (2015). Insights into low-latitude cloud feedbacks from high-resolution models. *Philosophical Transactions of the Royal Society A: Mathematical, Physical & Engineering Sciences*, 373(2054), 20140415. https://doi.org/10.1098/rsta.2014.0415
- Bretherton, C. S., & Blossey, P. N. (2014). Low cloud reduction in a greenhouse-warmed climate: Results from Lagrangian LES of a subtropical marine cloudiness transition. *Journal of Advances in Modeling Earth Systems*, 6(1), 91–114. https://doi.org/10.1002/2013MS000250
- Bretherton, C. S., Blossey, P. N., & Jones, C. R. (2013). Mechanisms of marine low cloud sensitivity to idealized climate perturbations: A single-LES exploration extending the CGILS cases. *Journal of Advances in Modeling Earth Systems*, 5(2), 316–337. https://doi.org/10.1002/jame.20019
- Ceppi, P., Brient, F., Zelinka, M. D., & Hartmann, D. L. (2017). Cloud feedback mechanisms and their representation in global climate models. WIREs Climate Change, 8(4), e465. https://doi.org/10.1002/wcc.465
- Ceppi, P., Hartmann, D. L., & Webb, M. J. (2016). Mechanisms of the negative shortwave cloud feedback in middle to high latitudes. *Journal of Climate*, 29(1), 139–157. https://doi.org/10.1175/JCLI-D-15-0327.1
- Ceppi, P., & Nowack, P. (2021). Observational evidence that cloud feedback amplifies global warming. Proceedings of the National Academy of Sciences, 118(30), e2026290118. https://doi.org/10.1073/pnas.2026290118
- Chen, Y.-W., Seiki, T., Kodama, C., Satoh, M., Noda, A. T., & Yamada, Y. (2016). High cloud responses to global warming simulated by two different cloud microphysics schemes implemented in the Nonhydrostatic Icosahedral Atmospheric Model (NICAM). *Journal of Climate*, 29(16), 5949–5964. https://doi.org/10.1175/JCLI-D-15-0668.1
- Cronin, T. W., & Wing, A. A. (2017). Clouds, circulation, and climate sensitivity in a radiative–convective equilibrium channel model. *Journal of Advances in Modeling Earth Systems*, 9(8), 2883–2905. https://doi.org/10.1002/2017MS001111
- Dufresne, J.-L., & Bony, S. (2008). An assessment of the primary sources of spread of global warming estimates from coupled atmosphere–ocean models. *Journal of Climate*, 21(19), 5135–5144. https://doi.org/10.1175/2008JCL12239.1
- Eyring, V., Bony, S., Meehl, G. A., Senior, C. A., Stevens, B., Stouffer, R. J., & Taylor, K. E. (2016). Overview of the Coupled Model Inter-comparison Project Phase 6 (CMIP6) experimental design and organization. Geoscientific Model Development, 9(5), 1937–1958. https://doi.org/10.5194/gmd-9-1937-2016
- Flatau, P. J., Walko, R. L., & Cotton, W. R. (1992). Polynomial fits to saturation vapor pressure. *Journal of Applied Meteorology*, 31(12), 1507–1513. https://doi.org/10.1175/1520-0450(1992)031<1507:PFTSVP>2.0.CO;2
- Gordon, N. D., & Klein, S. A. (2014). Low-cloud optical depth feedback in climate models. *Journal of Geophysical Research: Atmospheres*, 119(10), 6052–6065. https://doi.org/10.1002/2013JD021052
- Hartmann, D. L., Blossey, P. N., & Dygert, B. D. (2019). Convection and climate: What have we learned from simple models and simplified settings? Current Climate Change Reports, 5(3), 196–206. https://doi.org/10.1007/s40641-019-00136-9
- Hartmann, D. L., & Larson, K. (2002). An important constraint on tropical cloud-climate feedback. *Geophysical Research Letters*, 29(20), 12-1-12-4. https://doi.org/10.1029/2002GL015835
- Held, I. M., Hemler, R. S., & Ramaswamy, V. (1993). Radiative–convective equilibrium with explicit two–dimensional moist convection. *Journal of the Atmospheric Sciences*, 50(23), 3909–3927. https://doi.org/10.1175/1520-0469(1993)050<3909:RCEWET>2.0.CO;2
- Holloway, C., Wing, A., Bony, S., Muller, C., Masunaga, H., L'Ecuyer, T., et al. (2017). Observing convective aggregation. Surveys in Geophysics, 38(6), 1199–1236. https://doi.org/10.1007/s10712-017-9419-1
- Igel, M. R., Drager, A. J., & van denHeever, S. C. (2014). A CloudSat cloud object partitioning technique and assessment and integration of deep convective anvil sensitivities to sea surface temperature. *Journal of Geophysical Research: Atmospheres*, 119(17), 10515–10535. https://doi. org/10.1002/2014JD021717
- Ingram, W. (2010). A very simple model for the water vapour feedback on climate change. *Quarterly Journal of the Royal Meteorological Society*, 136(646), 30–40. https://doi.org/10.1002/qi.546
- Jakob, C., Singh, M., & Jungandreas, L. (2019). Radiative convective equilibrium and organized convection: An observational perspective. *Journal of Geophysical Research: Atmospheres*, 124(10), 5418–5430. https://doi.org/10.1029/2018JD030092
- Jeevanjee, N., & Fueglistaler, S. (2020). Simple spectral models for atmospheric radiative cooling. *Journal of the Atmospheric Sciences*, 77(2), 479–497. https://doi.org/10.1175/JAS-D-18-0347.1
- Jeevanjee, N., & Romps, D. M. (2018). Mean precipitation change from a deepening troposphere. Proceedings of the National Academy of Sciences, 115(45), 11465–11470. https://doi.org/10.1073/pnas.1720683115
- Jeevanjee, N., & Zhou, L. (2022). On the resolution–dependence of anvil cloud fraction and precipitation efficiency in radiative–convective equilibrium. *Journal of Advances in Modeling Earth Systems*, 14(3), e2021MS002759. https://doi.org/10.1029/2021MS002759
- Khairoutdinov, M. F., & Randall, D. A. (2003). Cloud resolving modeling of the ARM summer 1997 IOP: Model formulation, results, uncertainties, and sensitivities. *Journal of the Atmospheric Sciences*, 60(4), 607–625. https://doi.org/10.1175/1520-0469(2003)060<0607:CRMOTA>2.

STAUFFER AND WING 21 of 23



- Kodama, C., Ohno, T., Seiki, T., Yashiro, H., Noda, A. T., Nakano, M., et al. (2021). The Nonhydrostatic ICosahedral Atmospheric Model for CMIP6 HighResMIP Simulations (NICAM16-S): Experimental design, model description, and impacts of model updates. Geoscientific Model Development, 14(2), 795–820. https://doi.org/10.5194/gmd-14-795-2021
- Kuang, Z., & Hartmann, D. L. (2007). Testing the fixed anvil temperature hypothesis in a cloud–resolving model. *Journal of Climate*, 20(10), 2051–2057. https://doi.org/10.1175/JCLI4124.1
- Lau, K., Sui, C. S., Chou, M., & Tau, W. (1994). An inquiry into the cirrus-thermostat effect for tropical sea surface temperature. Geophysical Research Letters, 21(12), 1157–1160. https://doi.org/10.1029/94g100222
- McCoy, D. T., Hartmann, D. L., Zelinka, M. D., Ceppi, P., & Grosvenor, D. P. (2015). Mixed–phase cloud physics and Southern Ocean cloud feedback in climate models. *Journal of Geophysical Research: Atmospheres*, 120(18), 9539–9554. https://doi.org/10.1002/2015JD023603
- Miyakawa, O., Shaw, T. A., & Jansen, M. F. (2022). Quantifying energy balance regimes in the modern climate, their link to lapse rate regimes, and their response to warming. *Journal of Climate*, 35(3), 1045–1061. https://doi.org/10.1175/JCLI-D-21-0440.1
- Noda, A. T., Kodama, C., Yamada, Y., Satoh, M., Ogura, T., & Ohno, T. (2019). Responses of clouds and large–scale circulation to global warming evaluated from multidecadal simulations using a global nonhydrostatic model. *Journal of Advances in Modeling Earth Systems*, 11(9), 2980–2995. https://doi.org/10.1029/2019MS001658
- Ohno, T., Noda, A. T., & Satoh, M. (2020). Impacts of sub-grid ice cloud physics in a turbulence scheme on high clouds and their response to global warming. *Journal of the Meteorological Society of Japan. Ser. II*, 98(5), 1069–1081. https://doi.org/10.2151/jmsj.2020-054
- Ohno, T., Noda, A. T., Seiki, T., & Satoh, M. (2021). Importance of pressure changes in high cloud area feedback due to global warming. Geophysical Research Letters, 48(18), e2021GL093646. https://doi.org/10.1029/2021GL093646
- Ohno, T., & Satoh, M. (2018). Roles of cloud microphysics on cloud responses to sea surface temperatures in radiative–convective equilibrium experiments using a high–resolution global nonhydrostatic model. *Journal of Advances in Modeling Earth Systems*, 10(8), 1970–1989. https://doi.org/10.1029/2018MS001386
- Ohno, T., Satoh, M., & Noda, A. (2019). Fine vertical resolution radiative-convective equilibrium experiments: Roles of turbulent mixing on the high-cloud response to sea surface temperatures. *Journal of Advances in Modeling Earth Systems*, 11(6), 1637–1654. https://doi.org/10.1029/2019MS001704
- Po-Chedley, S., Zelinka, M. D., Jeevanjee, N., Thorsen, T. J., & Santer, B. D. (2019). Climatology explains intermodel spread in tropical upper tropospheric cloud and relative humidity response to greenhouse warming. *Geophysical Research Letters*, 46(22), 13399–13409. https://doi. org/10.1029/2019GL084786
- Randall, D. A., Wood, R. A., Bony, S., Colman, R., Fichefet, T., Fyfe, J., et al. (2007). Climate models and their evaluation. In S. Solomon, D. Qin, M. Manning, Z. Chen, M. Marquis, K. B. Avery, et al. (Eds.), Climate change 2007: The physical science basis. contribution of working group i to the fourth assessment report of the intergovernmental panel on climate change (pp. 596–662). Cambridge University Press.
- Reed, K. A., Silvers, L. G., Wing, A. A., Hu, I.-K., & Medeiros, B. (2021). Using radiative convective equilibrium to explore clouds and climate in the Community Atmosphere Model. *Journal of Advances in Modeling Earth Systems*, 3(12), e2021MS002539. https://doi.org/10.1029/2021MS002539
- Rieck, M., Nuijens, L., & Stevens, B. (2012). Marine boundary layer cloud feedbacks in a constant relative humidity atmosphere. *Journal of the Atmospheric Sciences*, 69(8), 2538–2550. https://doi.org/10.1175/JAS-D-11-0203.1
- Romps, D. M. (2014). An analytical model for tropical relative humidity. *Journal of Climate*, 27(19), 7432–7449. https://doi.org/10.1175/
- Seeley, J. T., Jeevanjee, N., Langhans, W., & Romps, D. M. (2019). Formation of tropical anvil clouds by slow evaporation. *Geophysical Research Letters*, 46(1), 492–501. https://doi.org/10.1029/2018GL080747
- Seeley, J. T., Jeevanjee, N., & Romps, D. M. (2019). FAT or FiTT: Are anvil clouds or the tropopause temperature invariant? *Geophysical Research Letters*, 46(3), 1842–1850. https://doi.org/10.1029/2018GL080096
- Sherwood, S. C., Webb, M. J., Annan, J. D., Armour, K. C., Forster, P. M., Hargreaves, J. C., et al. (2020). An assessment of Earth's climate sensitivity using multiple lines of evidence. Reviews of Geophysics, 58(4), e2019RG000678. https://doi.org/10.1029/2019RG000678
- Singh, M., & O'Gorman, P. (2012). Upward shift of the atmospheric general circulation under global warming: Theory and simulations. *Journal of Climate*, 25(23), 8259–8276. https://doi.org/10.1175/JCLI-D-11-00699.1
- Singh, M., & O'Gorman, P. (2015). Increases in moist-convective updraught velocities with warming in radiative-convective equilibrium. Quarterly Journal of the Royal Meteorological Society, 141(692), 2828–2838. https://doi.org/10.1002/qj.2567
- Stan, C., & Xu, L. (2014). Climate simulations and projections with a super-parameterized climate model. *Environmental Modelling & Software*, 60, 134–152. https://doi.org/10.1016/j.envsoft.2014.06.013
- Stauffer, C. L., & Wing, A. A. (2022). Cloud properties and changes in RCEMIP. Zenodo. https://doi.org/10.5281/zenodo.6323552
- Thorsen, T. J., Kato, S., Loeb, N. G., & Rose, F. G. (2018). Observation–based decomposition of radiative perturbations and radiative kernels. *Journal of Climate*, 31(24), 10039–10058. https://doi.org/10.1175/JCLI-D-18-0045.1
- Tompkins, A. M., & Craig, G. C. (1999). Sensitivity of tropical convection to sea surface temperature in the absence of large–scale flow. *Journal of Climate*, 12(2), 462–476. https://doi.org/10.1175/1520-0442(1999)012<0462:SOTCTS>2.0.CO;2
- Tsushima, Y., Iga, S.-i., Tomita, H., Satoh, M., Noda, A. T., & Webb, M. J. (2014). High cloud increase in a perturbed SST experiment with a global nonhydrostatic model including explicit convective processes. *Journal of Advances in Modeling Earth Systems*, 6(3), 571–585. https://doi.org/10.1002/2013MS000301
- Vial, J., Dufresne, J.-L., & Bony, S. (2013). On the interpretation of inter–model spread in CMIP5 climate sensitivity estimates. Climate Dynamics, 41(11–12), 3339–3362. https://doi.org/10.1007/s00382-013-1725-9
- Wexler, A. (1976). Vapor pressure formulation for water in range 0 to 100 C. A revision. *Journal of Research of the National Bureau of Standards Section A: Physics and Chemistry*, 80A(5 and 6), 775. https://doi.org/10.6028/jres.080A.071
- Wing, A. A., Emanuel, K., Holloway, C. E., & Muller, C. (2017). Convective self-aggregation in numerical simulations: A review. Surveys in Geophysics, 38(6), 1173–1197. https://doi.org/10.1007/s10712-017-9408-4
- Wing, A. A., Reed, K. A., Satoh, M., Stevens, B., Bony, S., & Ohno, T. (2018). Radiative–convective equilibrium model intercomparison project. Geoscientific Model Development, 11(2), 793–813. https://doi.org/10.5194/gmd-11-793-2018
- Wing, A. A., Stauffer, C. L., Becker, T., Reed, K. A., Ahn, M.-S., Arnold, N. P., et al. (2020). Clouds and convective self-aggregation in a multi-model ensemble of radiative-convective equilibrium simulations. *Journal of Advances in Modeling Earth Systems*, 12(9), e2020MS002138. https://doi.org/10.1029/2020MS002138
- Wu, X., & Moncrieff, M. W. (1999). Effects of sea surface temperature and large-scale dynamics on the thermodynamic equilibrium state and convection over the tropical western Pacific. *Journal of Geophysical Research*, 104(D6), 6093–6100. https://doi.org/10.1029/1998jd200116

STAUFFER AND WING 22 of 23



- Wyant, M. C., Bretherton, C. S., & Blossey, P. N. (2009). Subtropical low cloud response to a warmer climate in a superparameterized climate model. Part I: Regime sorting and physical mechanisms. *Journal of Advances in Modeling Earth Systems*, 1(3), 7. https://doi.org/10.3894/JAMES.2009.1.7
- Yue, Q., Kahn, B. H., Fetzer, E. J., Schreier, M., Wong, S., Chen, X., & Huang, X. (2016). Observation–based longwave cloud radiative kernels derived from the A-Train. *Journal of Climate*, 29(6), 2023–2040. https://doi.org/10.1175/JCLI-D-15-0257.1
- Zelinka, M. D., & Hartmann, D. L. (2010). Why is longwave cloud feedback positive? Journal of Geophysical Research, 115(D16), D16117. https://doi.org/10.1029/2010JD013817
- Zelinka, M. D., & Hartmann, D. L. (2011). The observed sensitivity of high clouds to mean surface temperature anomalies in the tropics: Temperature sensitivity of high clouds. *Journal of Geophysical Research*, 116(D23), D23103. https://doi.org/10.1029/2011JD016459
- Zelinka, M. D., Klein, S. A., & Hartmann, D. L. (2012). Computing and partitioning cloud feedbacks using cloud property histograms. Part I: Cloud radiative kernels. *Journal of Climate*, 25(11), 3715–3735. https://doi.org/10.1175/JCLI-D-11-00248.1
- Zelinka, M. D., Klein, S. A., Taylor, K. E., Andrews, T., Webb, M. J., Gregory, J. M., & Forster, P. M. (2013). Contributions of different cloud types to feedbacks and rapid adjustments in CMIP5. *Journal of Climate*, 26(14), 5007–5027. https://doi.org/10.1175/JCLI-D-12-00555.1
- Zelinka, M. D., Myers, T. A., McCoy, D. T., Po-Chedley, S., Caldwell, P. M., Ceppi, P., et al. (2020). Causes of higher climate sensitivity in CMIP6 models. *Geophysical Research Letters*, 47(1), e2019GL085782. https://doi.org/10.1029/2019GL085782
- Zelinka, M. D., Zhou, C., & Klein, S. A. (2016). Insights from a refined decomposition of cloud feedbacks. *Geophysical Research Letters*, 43(17), 9259–9269. https://doi.org/10.1002/2016GL069917
- Zhang, M. H. (2005). Comparing clouds and their seasonal variations in 10 atmospheric general circulation models with satellite measurements. *Journal of Geophysical Research*, 110(D15), D15S02. https://doi.org/10.1029/2004JD005021
- Zhou, C., Zelinka, M. D., Dessler, A. E., & Yang, P. (2013). An analysis of the short-term cloud feedback using MODIS data. *Journal of Climate*, 26(13), 4803–4815. https://doi.org/10.1175/JCLI-D-12-00547.1

STAUFFER AND WING 23 of 23